Revisiting Tropical Instability Wave Variability in the Atlantic Ocean using SODA reanalysis

Hatsue Takanaca de Decco[1], Audalio Rebelo Torres Junior[2] , Luciano Ponzi Pezzi[3], Luiz Landau[1]

[1]Laboratório de Métodos Computacionais em Engenharia (LAMCE), Instituto Alberto Luiz Coimbra de Pós-Graduação e Pesquisa em Engenharia, Universidade Federal do Rio de Janeiro, Postal Code 68.55, Rio de Janeiro – RJ, Brazil, 21941-972

[2]Laboratório de Modelagem de processos Marinhos e Atmosféricos (LAMMA), Departamento de Meteorologia , Universidade Federal do Rio de Janeiro, Rio de Janeiro, Brazil,ZIP Code: 21949-900

[3]Instituto Nacional de Pesquisas Espaciais (INPE), SERE II – OBT, Instituto Nacional de Pesquisas Espaciais – INPE, Av. dos Astronautas, 1758, São José dos Campos – SP, ZIP Code: 12227-010

Correspondence to: Audalio Rebelo Torres Junior (audalio.torres@gmail.com)

ABSTRACT. The spatial and temporal variability of energy exchange in Tropical Instability Waves (TIWs) in the Atlantic Ocean were investigated. A spectral analysis was used to filter the 5-day mean results from Simple Ocean Data Assimilation reanalysis spanning from 1958 to 2008. TIWs were filtered over periods of 15 to 60 days and between wavelengths of 4 and 20 longitude degrees. The main approach of this study was the use of bidirectionally filtered TIW time series as the perturbation fields, and the difference in these time series from the SODA total results was considered to be the basic state for energetics analysis. The main result was that the annual cycle (period of ~360 days) was the main source of variability of the waves, and the semi-annual cycle (period of ~180 days) was a secondary variation, which indicated that TIWs occurred throughout the year but with intensity that varies seasonally. Barotropic instability acts as the mechanism that feeds and extracts energy to/from TIWs as alternate zonal bands at equatorial Atlantic. Baroclinic instability is the main mechanism that extracts energy from TIWs to the equatorial circulation north of Equator. All TIW patterns of variability were observed at west of ~10ºW. The present study reveals new evidence regarding TIW variability and suggests that future investigations should include a detailed description of TIW dynamics as part of Atlantic Ocean equatorial circulation.

1 Introduction

A Tropical Instability Wave (TIW) is defined as a cusp-shaped oscillation of the equatorial thermal front that propagates westward. These waves are associated with the seasonal variability of the equatorial current system, and they are observed when the cold tongue (Figure 1) is well established (Chelton et al., 2000; Jochum et al., 2004a, Legeckis and Reverdin, 1987; Philander et al., 1986; Steger and Carton, 1991; Weisberg and Horigan, 1981). These westward waves have wavelengths ranging from 600 km to 2600 km and periods varying between 15 and 37 days in the Atlantic Ocean (Caltabiano et al., 2005; Chelton et al., 2000; Düing et al., 1975; Jochum et al., 2004b; Legeckis and Reverdin, 1987; Pezzi and Richards, 2003; Weisberg, 1984), and Athie and Marin (Athie and Marin, 2008) describes a wider range (periods of 15- 50 days). The formation process is the naturally generated instability of the equatorial zonal current system with alternating bands of eastward and westward flows

(Philander, 1976). In the Atlantic, the zonal flows at the top ocean layers are modulated by the coupled air-sea dynamics and have a strong seasonal cycle, as presented by Stramma and Schott (Stramma and Schott, 1999). The authors described the westward South Equatorial Current (SEC) as divided by three bands composed of northern, central and southern regions (the schematic surface circulation and its seasonality are depicted in their Figure 4 and not reproduced here). The eastward subsurface Equatorial Undercurrent (EUC) is at the Equator; it is strongest in its western portion, weakens downstream in the east Atlantic and is strongly associated with wind patterns (Philander, 1973). The strongest seasonality is observed for the eastward North Equatorial Counter Current (NECC), which is well developed during the northern fall and has its flow reversed to westward during the northern spring (Stramma and Schott, 1999). In this environment of intense shear with a sharp temperature gradient, TIWs are developed and maintained through barotropic and baroclinic instabilities, as will be discussed later in this section. Within the annual cycle of the equatorial Atlantic Ocean, TIWs constitute an adjustment feature in response to the zonal pressure gradient variation throughout the year, which drives energy from tropical regions to other regions of the planet (Cox, 1980; Weisberg and Horigan, 1981) . In this way, TIWs can be considered a fundamental component of the annual cycle of the equatorial Atlantic Ocean. Although many studies have examined energy conversions of intraseasonal and TIW-related variability (Grodsky et al., 2005; Jochum and Malanotte-Rizzoli, 2004; Philander, 1976, 1978; Philander et al., 1986; Proehl, 1998; von Schuckmann et al., 2008; Weisberg, 1984; Weisberg and Weingartner, 1988), there is no consensus to date regarding where (at the surface or at depth and at what latitude and longitude) and when (time of the year) energy exchanges are triggered or maintained in the Atlantic Ocean. Therefore, some aspects related to TIW physics that will be considered in this study are open questions. A brief review is presented to highlight some key points.

The dynamics of TIWs have been studied using various methodologies since they were first identified in the ocean during the late 1970s. TIWs were first recognized by Düing et al. (Düing et al., 1975) in the Atlantic during the time of the Equatorial Oceanographic Experiment (Düing, 1974), and the scientific community has since continued to investigate these waves. Düing et al. (Düing et al., 1975) used *in situ* temperature, salinity and velocity to study the meandering of zonal equatorial currents and westward propagating waves with 2600 km of wavelength and period of 16 days. Based on these observations, Philander (Philander, 1976) presented the first hypothesis concerning the occurrence of TIWs, associating the natural instabilities of equatorial zonal currents with the alternate bands of eastward and westward flows. Philander showed that according to ageostrophic dynamics, when beta effects become important, the divergence enhances the inertial stability of eastward currents and destabilizes westward flows. The barotropic instability resulting from the zonal shear between the SEC and NECC would thus be a TIW-triggering process with a rapid growth rate. Weisberg's observation-based studies in the 1980s in the Atlantic (Weisberg, 1979, 1984, 1985; Weisberg and Horigan, 1981; Weisberg and Weingartner, 1988) greatly contributed to the understanding of the main characteristics

and seasonality of TIWs. Despite the considerable advance in TIW characterization made in those early studies, including Reynolds' stresses calculation, the sparse *in situ* data distribution did not allow for the use of a bidirectional filter to properly isolate the spatial and temporal frequencies and period bands of the waves. This fact most likely has contributed to the influence of other seasonal oscillations than TIWs on the equatorial Atlantic, though the filtered signals were most likely highly TIW dominated. Weisberg and colleagues observed that the strongest activity associated with TIWs occurred from July to September at the Equator and were generated by barotropic instabilities at the anticyclonic shear (n.h.) between the SEC and NECC and within the SEC (cyclonic shear). Using numerical modeling, Philander et al. (Philander et al., 1986) showed that the barotropic instability between the SEC and NECC from the surface to 50 meters at 28ºW at the Equator was the main generation mechanism, thus corroborating Weisberg (Weisberg, 1984). Philander et al. (Philander et al., 1986) also showed that TIWs extract potential energy from the main currents. The present study suggests that due to the distinct methodologies applied to observed data and model results over the years, the results are ambiguous or there is some unknown TIW variability, as Weisberg and Weingartner (Weisberg and Weingartner, 1988), Proehl (Proehl, 1998) and Grodsky et al. (Grodsky et al., 2005) have since contradicted those earlier studies and concluded that the anticyclonic shear of SEC/NECC was not important for TIW generation. Conversely, these more recent studies found that cyclonic shear within the SEC just north of Equator is the main process involved in energy conversion and the shear between the SEC and EUC is also an energy source. More recently, the study of TIW energetics conducted by von Schuckmann et al. (von Schuckmann et al., 2008) corroborated both hypotheses (SEC/NECC and SEC/EUC shear). Im et al. (Im et al., 2012) also evaluated TIW variability (in the Pacific) using model results and energetic analysis. However, the authors' filtered TIWs used on eddy kinetic energy equation was a 50-day high-pass-filtered time series, and the mean state considered was the monthly mean. None of the above-cited authors completely isolated the TIW signal from their data/model results. Appropriate filtering is a fundamental aspect to be considered because other intraseasonal oscillations can be included in the analysis. There is some discussion regarding wave type at the identical spectral band of TIWs, which, for instance, occurs in the region east of 10ºW in the Guinea Gulf area, and considerations regarding the spatial limits of TIWs. This is an longstanding discussion see Weisberg et al. (Weisberg et al., 1979), with some recent studies regarding the intraseasonal variability along the equatorial Atlantic and Guinea Gulf region, e.g., (Athie and Marin, 2008; Bunge et al., 2007; Guiavarch et al., 2009). Similarly, in the western region, at approximately 30ºW, there is a concomitant occurrence of short Rossby waves with spectral characteristics similar to those of TIWs, as shown by Polito and Sato (Polito and Sato, 1029). These authors speculated that instability processes might also generate these short waves. Thus, these papers show the difficulty in defining spatial limits for the occurrence TIWs in the Atlantic, and this result can be attributed to the methodologies applied thus far. Additionally, distinct types of waves identified by filters will surely lead to distinct results, as argued by Lyman et al. (Lyman et al., 2007).

However, Caltabiano et al. (Caltabiano et al., 2005) successfully isolated (using spatial and temporal filters) TIW variability on satellite SST and defined the region of highest variability as being between 1ºN and 2ºN and between 25ºW and 10ºW in the Atlantic from January 1998 to December 2001.

Broadening the conception of TIWs as an equatorial mesoscale feature and their role in the oceans, these waves can be considered as a "non-linear feature modulated by the linear processes of zonal pressure gradient adjustment," as stated by Weisberg and Weingartner (Weisberg and Weingartner, 1988). In comparison, Weisberg and Weingartner (Weisberg and Weingartner, 1988) showed that the rates of energy conversion by barotropic instability relative to TIWs in the Atlantic are similar to the levels observed for western boundary current energy exchange. Baturin and Niiler (Baturin and Niiler, 1997) also noted that the kinetic energy perturbation during TIW season is one of the most intense in the world's oceans. Previously, Cox (Cox, 1980) observed that these waves reduced the perturbation energy accumulation in the shallower layers of the oceans, and Weisberg and Horigan (Weisberg and Horigan, 1981) considered TIWs to have a stabilizing effect on the oceans because the waves are responsible for redirecting energy from the upper equatorial oceans to deeper layers (Weisberg, 1984) and high latitudes (Farrar, 2011). Davey et al. (Davey et al., 2000) observed that a consistent representation of the upper ocean equatorial mixing and circulation is imperative to avoid amplified systematic errors (cold bias in SST) in coupled models of climate reproduction, since TIWs have important role in the atmosphere (Seo et al., 2007). The role of TIWs in climate modeling was addressed by Pezzi and Richards (Pezzi and Richards, 2003), Jochum et al. (Jochum et al., 2004a; Jochum and Malanotte-Rizzoli, 2004), Seo et al. (Seo et al., 2006) and Ham and Kang (Ham and Kang, 2011). In particular, Ham and Kang (Ham and Kang, 2011)obtained improved results for prognostic simulations using coupled models incorporating the variability of Pacific TIWs.

Finally, TIW activity is described as having strong seasonality (Jochum et al., 2004a). The onset of waves is generally observed in May (Jochum and Malanotte-Rizzoli, 2004) or June (Grodsky et al., 2005) and lasts until September (Grodsky et al., 2005; Weisberg, 1984). However, TIW activity has also been observed outside the range of those months during some years (Bunge et al., 2007; Perez et al., 2012). Again, this discussion and distinct characteristics might be associated with different methods of filtering data/model results only in time or space frequency bands or high TIW variability. Using a bidirectional filter applied to remotely sensed sea surface temperature (SST), Caltabiano et al. (Caltabiano et al., 2005) observed TIW seasonality from 1998 to 2001, which varied from year to year. Perez et al. (Perez et al., 2012) also used satellite data with temporal and zonal band-pass filter to study TIW variability in the Atlantic and found peak TIW variance during summer months. The main conclusion of these studies introduces a paradigm: why would TIWs only occur during some months if their role is to drive excess of energy from the equatorial region?

In the present study, we aimed to study the TIW variability in the Atlantic Ocean and revisit the discussion of TIW generation and propagation processes. Energetic analysis was applied to the 5-day

mean results of Simple Ocean Data Assimilation (SODA) Reanalysis (Carton and Giese, 2008) version 2.1.6, for the period of 1958 to 2008. The use of a reanalysis as a long time series lead to a more consistent representation of seasonal time scales due to the repetition of dynamic cycles. This study applied a twofold approach: a bidirectional (period and wavelength) band pass filter was used to extract the TIW signal, and this field was considered as the perturbation, and a transient (time-dependent) basic state was defined, both for energetics. It will be shown that this methodology maintains TIW signal in a manner similar to that reported by Pezzi and Richards (Pezzi and Richards, 2003), Caltabiano et al. (Caltabiano et al., 2005) and Pezzi et al. (Pezzi et al., 2006). Consistent advancements regarding TIW physics and dynamics will be achieved with the employment of this methodology.

Details regarding SODA simulation data processing and filtering are provided in the Methodology section. In Section 3, the filtered data are described and discussed and the main patterns of intraseasonal and TIW variability are identified. Subsequently, a comparison of the spectral characteristics for the filtered data is performed. Finally, the main conclusions are summarized in Section 4.

2 METHODOLOGY

2.1 SODA and TMI data

SODA is a multi-institutional project for reconstituting past ocean states using ocean modeling conducted mainly by the Department of Atmospheric and Oceanic Science at Maryland University. Previously to the SODA version 2.1.6 used in this study, long-term climatic ocean simulations have been performed and improved (James Carton, 2011, personal communication).

The ocean model of SODA was the Parallel Ocean Program (POP) (Carton and Giese 2008). POP is a Bryan-Cox-Semtner (from Geophysical Fluid Dynamics Laboratory, Princeton University)-derived model, and at Los Alamos National Laboratory, this model has been adapted for massively parallel computing to solve the equations. A free sea surface height (SSH) formulation was included (Smith et al. 1992). POP for SODA simulations has global coverage with a spatial resolution of 0.25º x 0.4º and 40 vertical levels with 10 meter spacing of the surface levels (Carton and Giese, 2008). The model was initialized with hydrographic information from the World Ocean Database 2005 (Johnson, 2006) developed and distributed by NOAA's National Oceanographic Data Center (NODC). A 1/30º ocean topography was used to generate the bottom boundary condition (Carton and Giese, 2008). A non-local K-profile parameterization (KPP scheme) was adopted for vertical mixing and a biharmonical mixture for horizontal mixing (Carton and Giese, 2008). Atmospheric data from the ECMWF (European Centre for Medium-Range Weather Forecast) ERA-40 reanalysis were used for the surface fluxes, covering the period 1958 to 2001. From 2002 to 2008, the database was changed to ERA-Interim (Czeschel et al., 2011). The SODA dataset was obtained for the period 1958 to 2008 as a 5-day average with a horizontal resolution of 0.5º at http://soda.tamu.edu/assim/SODA_2.1.6/5DAY.

SODA data have been used to investigate TIWs by Soon-II (An Soon-II, 2008; Soon-II, 2008) in the Pacific Ocean. An ocean reanalysis product such as SODA is useful for studying the processes and interannual variability considering its reasonable long time span (Dewitte et al., 2008; Du and Qu, 2010; Schoenefeldt and Schott, 2006). Nonetheless, a comparison between the filtered SODA surface temperature and satellite sea surface temperature (SST) was performed to verify the representation of main TIW pattern by SODA and is presented in the next section. The SST dataset used was a merged product derived from measurements of the Tropical Rainfall Measuring Mission Microwave Imager (TMI) and the Advanced Microwave Scanning Radiometer (AMSR-E). TMI and AMSR-E data are produced by Remote Sensing Systems and sponsored by the NASA Earth Science MEaSUREs DISCOVER Project and the AMSR-E Science Team. The data are available at www.remss.com. The SST data have a spatial resolution of ¼º, and for the present study, the time series was 6 years, from 2003 to 2008, and was obtained as daily fields. The daily SST product was used for comparison with the 5-day SODA results to avoid underestimation of the TIW signal. The filtering method applied to both datasets (SODA and satellite SST) is described in the following section.

2.2 Data pre-processing and filtering

SODA fields of temperature, salinity, SSH, zonal and meridional velocity components for the tropical Atlantic region (from 20ºN to 20ºS and 40ºW to 15ºE with 40 vertical levels) for the entire period (1958-2008) were treated to remove spurious data (there were some not-a-number (NaN) data along the SODA 2.1.6 5-day mean database). Additionally, a vertical velocity component was calculated using the continuity equation, and the density fields were calculated using a MatLab seawater script for density using the non-linear equation of state (Fofonoff and Millard, 1983; Millero et al., 1980). The data were organized as longitude x time matrices to perform the filtering. To filter the data in both dimensions (spatial and temporal), a Fourier 2D directional filter was designed using a two-dimensional fast Fourier transform (2DFFT). A band pass filter was applied to the data matrices to retain periods from 15 to 60 days and wavelengths from 4º to 20º of longitude, which was a slightly wider range than Caltabiano et al. (Caltabiano et al., 2005) considered. Here, these filtered data will be called TIW data.

For dominant wavelength and period estimation, a spectral analysis using the fast Fourier transform was applied to the TIW data. To calculate wave speed, the Radon Transform technique (Challenor et al., 2001; Deans, 1983)was also applied because it has been successfully used by Caltabiano et al. (Caltabiano et al., 2005), Pezzi et al. (Caltabiano et al., 2005) and Athié and Marin (Athie and Marin, 2008) to study TIWs and intraseasonal variability.

2.3 Energy budget

Energy transferences related to TIWs have been studied using time series decomposed into the (temporal) mean state and its deviation by, e.g., Weisberg and Weingartner (Weisberg and Weingartner, 1988), Masina et al. (Masina et al., 1999), Pezzi and Richards (Pezzi and Richards, 2003), Jochum et al.

(Jochum et al., 2004b), von Schuckmann et al. (von Schuckmann et al., 2008), among others. In all these studies, the mean state was considered to be the time-averaged fields at either monthly or yearly time scales. However, because we have spatially and temporally filtered TIW signals from the SODA time series, the present study adopted a distinct definition for the flux decomposition. To analyze the TIW energy as a perturbation, the basic state as a subtraction of SODA total fields minus TIW filtered data was considered, according to the following formula:

$$t' = T - T_b \quad (1),$$

where T is the 5-day average temperature directly extracted from SODA, T_b is the temperature for the basic state and t' is the filtered (TIW) temperature. The identical decomposition was performed for the SODA available (salinity, zonal and meridional velocity components and SSH) and derived (density, pressure and vertical velocity component) fields. Thus, the time evolution of energy transformations between TIWs and the basic state was analyzed, which included all intraseasonal energy that could interact with TIWs.

Orlanski and Katzfey (Orlanski and Katzfey, 1991) used transient "mean" state in energy budget analyses to study the energetics of cyclonic waves in the atmosphere; however, the authors justified the mean state transience by adding a forcing term related to the non-steadiness of the time mean in the mean state of the momentum equation. Subsequently, Lackmann et al. (Lackmann et al., 1999) applied a similar approach with an unsteady background state for the energetic analysis of atmospheric cyclones. Similar to both studies, the eddy kinetic energy (EKE) equation used here remains identical with identical energy conversion terms, although we considered a transient basic state. However, for clarification, the system of energy equations was derived to show the responsible terms for the basic state transience.

Following a similar approach used by Orlanski and Katzfey (Orlanski and Katzfey, 1991), we derived the kinetic energy equation using the classical method (by subtracting the time mean of the momentum equations from the total momentum equation). Similar to the approach taken by these authors, we took into account the non-steadiness of the basic state. The full EKE derivation under such considerations is described in the appendix.

The analysis was conducted in this study by performing a calculation of these energy conversion terms, and their temporal and spatial patterns are described in the following section.

3 RESULTS AND DISCUSSION

The filtering method was applied for the tropical Atlantic domain from SODA. Before the main discussion, three spectra are shown in Figure 2 to elucidate the variability referred in the subsequent sections. The power spectra for the total and basic states and TIW time series of temperature for a grid point of 0.25ºN and 20.25ºW are presented. This location was chosen to because it is, on average, at the central point of maximum variability observed with the standard deviation fields showed on Figure 5

(described later on). The TIW spectrum (Figure 2c) clearly shows the filtered frequency band. In the total and basic state spectra (Figures 2a and b, respectively), the highest variability was at the annual (~ 360 days) and semi-annual (~ 180 days) periods. A similar pattern was observed for spatial spectra (wavelength) but it is not shown.

3.1 TIWs in SODA and satellite data

The temperature at the first vertical model layer was compared with TMI/AMSR-E SST to evaluate the reliability of temperature representation by SODA. Figure 1 has two panels showing daily satellite SST for 16 August 2006, and a five-day average SODA for 12 to 17 August 2006. TIWs were observed with distinct wavelengths for both datasets. In Figure 3, these differences are shown with the longitude-time plots of temperature along the latitude of 0.25ºN (Figures 3a, b and c) for both (satellite and model). An underestimation of TIW amplitude in the ocean model (Figure 3b) was observed when compared with the satellite data (Figure 3a). TIW phase velocities were also distinct (Figure 3c) during the strongest season of TIWs in 2003. However, TIW variability was quite well reproduced. Spectral characteristics, such as the dominant periods and wavelengths, were calculated and analyzed from 2003 to 2008 and are shown in Table 1. Overall, TIWs were shorter in the satellite SST than in the SODA reanalysis, whereas their periods were approximately identical. These differences were expected because of the two distinct methods of SST estimation. However, TIW physics were well represented in the SODA simulation, and thus the related processes could be studied. There is a concern in the literature regarding the influence of data assimilation procedures on the TIW representation (see Imada et al. (Imada et al., 2013) for example) and whether these procedures can dampen or intensify TIWs. However, we are not aware of any specific study regarding this influence on TIWs in the SODA.

3.2 TIW data and variability

In this section, only results using the filtered SODA data, which we call TIW data, are discussed. The fields of temperature, salinity and the three velocity components in the first vertical model layer (for instance, 12 to 17 August 2006) used to calculate energy conversion terms between the basic state and TIW data are shown in Figure 4. In this illustration, the basic state and TIW data are plotted showing the same wave train shown in Figure 1. In the basic state maps (the middle panels of Figure 4), TIW oscillations (right panels in Figure 4) might not have been totally removed from the total fields (left panels in Figure 4). This fact can be attributed to the spectral range used in the filter (15- to 60-day periods and 4º to 20º degrees of longitude for wavelength), which may not have captured the entire spectrum of TIW characteristics in the SODA results. Nonetheless, we observe that the main TIW pattern was successfully filtered out from the total fields. Notably, the oscillations observed in the total temperature field (Figure 4a) east of 10ºW were not TIWs because these oscillations were also observed in the temperature basic state field (Figure 4b). In general, at least for this short analysis (in this case, 12 to 17 August 2006), spatially, TIWs start at approximately 10ºW, propagating to west of this position.

The region of maximum variability of TIWs is shown in Figure 5. The maps of the standard deviations of temperature (Figure 5a), salinity (Figure 5b), the three velocity components (Figures 5c, d and e) in the first vertical layer and sea surface elevation (Figure 5f) show that the maximum variability was mainly west of 10ºW to approximately 40ºW. However, certain variables exhibited distinct patterns. The maximum temperature variability was shifted eastward between the longitudes of 35ºW and 5ºE. This spatial distribution was similar to that observed by Athié and Marin (Athie and Marin, 2008). Additionally, the maximum temperature variability of their intraseasonal filtered SST (approximately 0.7ºC) was higher than the maximum estimated here (approximately 0.25ºC). This result shows that TIW temperature anomalies were a dominant source of variability in the central equatorial Atlantic, likely modulated the seasonal cold tongue. The salinity also showed a region of high variability coincident with that observed for temperature but zonally shorter. However, a maximum of salinity variability was observed around the African coast in the Southern Hemisphere (Figure 5b). This maximum may have masked the central equatorial Atlantic maximum. Recently, Lee et al. (Lee et al., 2012) showed that the TIW signature in the Pacific Ocean using satellite salinity fields has characteristics that are distinct from those examined based on satellite temperature, which suggests that different types of waves occur, thermodynamically decoupling the TIW signatures revealed by salinity fields and those revealed by temperature. The velocity fields (Figures 5c, d and e) exhibited two regions of high variability. The stronger variability was concentrated within the low-latitude degrees around the Equator, slightly shifted to the north, and a second area was in the Southern Hemisphere between 32ºW and 15ºW. Finally, the SSH (Figure 5f) exhibited a completely different pattern, which was most likely associated with large-scale oceanic variability, and these features were not investigated in this study. Athié and Marin (Athie and Marin, 2008) evaluated the standard deviations of the intraseasonal variability observed in the equatorial Atlantic Ocean using 10- to 50- day filtered sea level anomaly (SLA) time series from AVISO. The authors observed a maximum value of 2.1 cm of variability, which is much higher than values in Figure 5f. Due to the wider spectral band used to filter the time series, an even wider variability was observed by von Schuckmann et al. (von Schuckmann et al., 2008), also using SLA from AVISO, with a maximum variability of 5 cm. This discrepancy was strongly associated with the distinct filtering processes used in the three studies as well as the methods of reanalysis.

The study of the main ocean model variables associated with TIWs is important to describing the waves' signatures and comparing them to those reported in previous studies. However, the kinetic energy is also an important parameter in the study of TIW variability and is investigated here. In this study, as described in Section 2.3, TIWs were considered to be the perturbation field for the energetics analysis presented in the next section. Its kinetic energy is called TIW kinetic energy (TIW KE). A EKE calculation similar to that used by Weisberg and Weingartner (Weisberg and Weingartner, 1988) was performed. The model grid location nearest to the point where data were collected and studied by these authors was chosen, and the calculated TIW KE was plotted (Figure 6) to enable a comparison with

their values and description (their Figure 5). Weisberg and Weingartner (Weisberg and Weingartner, 1988) used perturbation around the 25-day average data on first 10 meters (depth). We observed some seasonal variability in the TIW KE (Figure 6), but it was clearly not as marked as the seasonality observed by Weisberg and Weigartner (Weisberg and Weingartner, 1988) Instead, there is considerable seasonal variation in strength of the TIW KE associated with phases of the absence/presence of the waves. This pattern was evident on maps of the three-month average statistical mean (Figure 7) and standard deviation (Figure 8) of TIW KE using the same units of Weisberg and Weingartner (Weisberg and Weingartner, 1988) The TIW KE observed here was three orders of magnitude higher than that reported by Weisberg and Weingartner (Weisberg and Weingartner, 1988) based on perturbation EKE. This difference can be attributed to distinct methodologies used (observed data *versus* model results and distinct filtering methods). The standard deviation (Figure 8) revealed that the main variations in EKE are just north and south of the Equator and between approximately 27ºW and 20ºW from September to February and between around 32ºW and 25ºW during the rest of year. Additionally, the TIW KE mean found in the present study is very similar to the results found by von Schuckmann et al (von Schuckmann et al., 2008) see their figure 1c, though the considerations regarding the different methodologies employed still apply. Besides the comparison with previous studies, important to notice is that the EKE was almost constant at seasonal scale (Figure 8). This is a striking result of the present study and the following analysis will emphasize this first evidence.

To evaluate TIW activity and spatial and temporal variability during 51 years of simulation, four indexes were created. For this calculation, the absolute values of the filtered SODA 5-day mean time series (TIW data) of temperature, salinity, the three velocity components and sea surface elevation were used. Each index value was calculated as the arithmetic mean of the sum of the absolute values of TIW data, for each variable over the box each limit (Figure 1b), for each time-step (5-day average). Absolute values were used to represent the real TIW intensity and evaluate its occurrence trough the time. Additionally, these limits were chosen based on the standard deviation analysis performed in the previous section. All index boxes were within the latitudes of 4.45ºS and 4.75ºN. The East Index (EI) was from 10.25ºW to 9.75ºE, the West 1 Index (W1I) was from 20.25ºW to 10.25ºW, the West 2 Index (W2I) was from 30.25ºW to 20.25ºW and the West 3 Index (W3I) was from 40.25ºW to 30.25ºW.

To identify the main temporal oscillations related to each region (index) and variable, a simple spectral analysis was applied to the time series for each index, and the results are shown in Figure 9. The interannual variability was not investigated here (a recent reference for this subject is the study of Perez et al. (Perez et al., 2012). The strongest variability observed was the annual cycle for all variables, except for meridional velocity in the eastern region (Figure 9d), along the entire equatorial extension. This result did not support the pattern previously observed for TIWs (Bunge et al., 2007; Grodsky et al., 2005; Jochum et al., 2004b; Weisberg, 1984), perhaps because the annual periodicity was not investigated by those authors. The work of Caltabiano et al. (Caltabiano et al., 2005) was the only one

in which the TIW signal was apparently represented throughout the year for the Atlantic (it was not possible to confirm this finding because the color scale used in their figure make it unclear). These authors also used a directional filter, which is a fundamental methodology for more effectively isolating TIWs. The fact that the annual cycle was the strongest indicates that TIW anomalies occurred throughout the year but became visible (and most intense) in the surface temperature fields only with the appearance of the seasonal cold tongue. We also speculate that because of the absence of the annual cycle peak in the meridional velocity time series spectrum for the EI and because the EI is always the weakest index in the spectral analysis (Figure 9), the annual cycles of temperature, salinity, SSH and zonal velocity at this equatorial area was most likely related to other phenomena than TIWs, as discussed by Weisberg et al. (Weisberg et al., 1979) and Philander (Philander, 1977). There is no consensus regarding whether the intraseasonal variability in the Gulf of Guinea is a result of TIWs (Athie and Marin, 2008; Bunge et al., 2007; Guiavarch et al., 2009), and further studies regarding its dynamics will help to elucidate this hypothesis.

A semi-annual cycle (180 days) was identified for all the western indexes for all variables (Figure 9), and this spectral peak was never stronger than the annual peak. Based on previous studies using intraseasonally (not only TIWs) filtered time series with limited spatial extensions and shorter time spans from observed data or model results, the expected TIW seasonality was the 4- to 5-month variability. The longer time series used showed that this was a secondary variation. This 180-day variability was also a new result. The characteristics of TIWs have not previously been studied using ocean reanalysis model results with all variables. The present analysis revealed and reinforced the intense seasonality of TIWs, but this was not the dominant form of variability.

The weakest TIW oscillation observed in the index spectra (Figure 9) was approximately 120 days. This periodicity was observed for temperature (Figure 9a) and zonal velocity (Figure 9c) in the middle equatorial region (for W2I and W1I indexes). For the meridional velocity, this peak occurred in the W3I and W2I index regions. Because of this scarcity, the 120-day variability observed in the series was not associated with TIW dynamics.

For these five spectra, the TIW variability was always more intense in the middle equatorial area between 30ºW and 10ºW. This result corroborates those reported by Weisberg and Weingartner (Weisberg and Weingartner, 1988), Jochum et al. (Jochum et al., 2004b), Caltabiano et al. (Caltabiano et al., 2005) and Athié and Marin (Athie and Marin, 2008)for the Atlantic Ocean. In fact, the analysis showed that TIW anomalies were also observed throughout the year and with interannual variations.

3.3 TIW energy exchange

In this section, the energy exchanges of TIWs are discussed. The results shown for the barotropic Kelvin-Helmholtz

$$\rho_0 \left[u' \left(u' \frac{\partial u_b}{\partial x} + v' \frac{\partial u_b}{\partial y} \right) - v' \left(u' \frac{\partial v_b}{\partial x} + v' \frac{\partial v_b}{\partial y} \right) \right],$$

$\rho_0\left[u'w'\frac{\partial u_b}{\partial z}+v'w'\frac{\partial v_b}{\partial z}\right]$ and baroclinic $\left(-gr'w'\right)$ energy conversion terms were averaged for the whole reanalysis time spam. The reader is referred to the appendix for the kinetic energy equation. The maps of the means (left panels) and standard deviations (right panels) of the three forms of energy conversion are plotted in Figure 10. The upper maps represent the barotropic (Figures 10a and b), the middle panels represent the Kelvin-Helmholtz (Figures 10c and d), and the bottom maps represent the baroclinic (Figures 10e and f) energy conversion terms of Eq. (15). In general, all energy conversions occurred between ~ 7ºS and 5ºN. The barotropic energy exchanges related to the horizontal shear (Figures 10a) played the major role. Barotropic energy conversion trough horizontal shear was important for the generation and propagation of TIWs (associated with positive conversion terms values, i.e. TIWs extracting energy from basic state) south of the Equator for the entire equatorial extension (Figure 10a). South of the Equator, the negative values characterized the energy transference from TIWs to the basic circulation. This could be related to some instability of SEC south (Jochum and Malanotte-Rizzoli, 2004), but it would be an analysis covering more aspects of the dynamics of the equatorial circulation and this is not main scope of this study. For the vertical shear (Kelvin-Helmholtz conversion, Figure 10c), the mean pattern was the gain of energy by the waves from the basic state along the entire equatorial extension. There was also a second zonal extension of positive values for Kelvin-Helmholtz between 5ºS and 2ºS from 35ºW to 10ºW. For both barotropic energy conversions, the high values of standard deviations (Figure 10b and d) characterized the mean values as a non-significant pattern for the Equator. Also, these results suggested that the end of the trajectory of TIWs in the Atlantic Ocean was between 40ºW and 35ºW. Finally, for the baroclinic energy conversions (Figure 10e), there was a pattern of TIWs driving energy to the basic state just north of the Equator, with the opposite result occurring south of the Equator. However, main region of mean negative values north of the Equator was associated with a high standard deviation (Figure 10f), which was related to a high variability in this area. A similar meridional distribution of the mean baroclinic conversions was observed by von Schukmann et al. (von Schuckmann et al., 2008). We conclude that west of 10ºW and north of the Equator, the main generating mechanism for TIWs was barotropic conversion due to horizontal and vertical flow shears and that TIWs drive energy back to the equatorial circulation trough baroclinic conversion. South of the Equator, a less intense TIW signal is generated and kept trough baroclinic and Kelvin-Helmholtz energy conversion and the waves drive energy back to the equatorial circulation trough horizontal shear. This pattern is quite zonally defined, which suggests almost steady conditions (there is slight variance in negative values in the region of NECC, but it is not visible at this color scale) of horizontal shear occurring on the equatorial band and its importance to energy cascade, as discussed by Weisberg and Horigan (Weisberg and Horigan, 1981). The seasonality for each energy conversion term was further explored but it is not shown because of the low variance for the three types of energy conversion, which reinforces this hypothesis of Weisberg and Horigan (Weisberg and

Horigan, 1981). The baroclinic conversion term exhibited a zonal region from the Equator to almost 4ºN, where TIWs lose energy to the basic state flow.

The quantities of energy conversion terms observed in this study were not comparable with any previous study of the generation processes of TIWs probably because a directional filter was used in this study to isolate TIWs from time series. Pezzi and Richards (Pezzi and Richards, 2003) used a similar methodology; however, their simulation was climatological and examined the Pacific Ocean. The authors also demonstrated that their choice to mixing schemes in model configuration strongly influenced the occurrence of TIWs (Pezzi and Richards, 2003); thus, differences in spatial and temporal variability and quantities were expected. However, some considerations can be made regarding patterns of positive and negative values, even for studies focusing on equatorial intraseasonal variations. In the barotropic instability seasonal maps of von Schuckmann et al. (von Schuckmann et al., 2008), a distinction between positive and negative values between the Southern and the Northern Hemispheres was observed (their Figure 8). The time mean barotropic conversion calculated by Masina et al. (Masina et al., 1999) also exhibited a similar spatial distribution with respect to the Equator. The time mean of barotropic (horizontal) energy conversion time series (Figure 10a) also presented this alternate pattern near the Equator. This also draws attention to the importance TIWs have to the equilibrium state of energy at the equatorial Atlantic.

The spectral character of energy conversion is shown in Figure 11. For the three types of instability, the annual cycle was the strongest form of variation, followed by the semi-annual cycle. This result corroborates the earlier analysis with the index variables, thus reinforcing that TIWs occur throughout the year with different modes of variability.

4 SUMMARY AND CONCLUSIONS

In this paper, the spatial and temporal variability of TIWs in the Atlantic Ocean was investigated with a focus on energy conversions. The 5-day mean results of the SODA ocean reanalysis version 2.1.6 spanning from 1958 to 2008 were used. Time series of all the available variables (SSH, temperature, salinity, zonal and meridional velocities, and also estimated vertical velocity) were filtered using a directional band-pass filter that maintained oscillations at 15- to 60-day periods and wavelengths of 4- to 20-degrees. Then, the classical energetic analysis was applied to these filtered time series containing TIW anomalies. A basic state was considered as being the total SODA time series subtracted from the anomalies, and the energy conversion terms for the barotropic and baroclinic instabilities were calculated.

Despite the reasonable caution regarding mathematical and physical approximations used in ocean modeling, the results presented here are useful to provide new insights into TIWs. Some previous studies (Jochum et al., 2004b; von Schuckmann et al., 2008)have also used ocean models to study (temporal) filtered TIW generation processes in the Atlantic Ocean. However, a directionally filtered

time series of TIWs to more concisely investigate wave generation had not been presented in the literature. When TIWs are isolated according to period and wavelength, their dynamics become free from the "noise" of other intraseasonal oscillations. Otherwise, only temporal band pass filtered time series in the equatorial Atlantic retain both TIWs and Kelvin waves (Decco, 2011; Han et al., 2008; Jiang et al., 2009; Katz, 1997; Qiao and Weisberg, 1995, 1998). Decco (Decco, 2011) observed interactions with Kelvin waves when TIWs were only filtered in the temporal band frequency, which significantly altered the amplitudes of TIWs. Therefore, the "pure" dynamics of TIWs remain an almost undescribed and greatly important subject to be investigated.

TIWs are classically defined as seasonal westward oscillations that appear as a result of intense zonal currents shear and the cold-water intrusion at equatorial latitudes, commonly observed from May to September. The spatial distribution of the maximum variation for each analyzed variable was distinct as a function of TIW dynamics. In general, the main variation was within the latitudes of 5ºS and 5ºN and from 40ºW to arpproximately 10ºW, which corroborated previous studies (Athie and Marin, 2008; von Schuckmann et al., 2008). The temporal variation of anomalies was analyzed using indexes of average amplitudes, shown inside the boxes in Figure 1b. The spectral characteristics of the spatial average of TIW anomalies through the analysis of indexes showed important variability patterns.

An interesting series of evidence shows that TIWs have frequency the cycle of ~360 days mode of occurrence, which may be responsible for the almost steady conditions observed for the waves in the present study. The seasonal pattern of TIW KE calculated with the filtered time series of the SODA reanalysis suggests that the waves signal are present the entire year, with low variance. Similar characteristics were observed for the seasonality of the three types of energy conversions. The energy transfers occurs mainly between 6ºS and 4ºN (see Section 3.3 for details), and the most energetic type is the horizontal barotropic instability. Baroclinic instability is the main responsible for the energy flow back from TIWs to the equatorial circulation, from the Equator to 4ºN. This new result corroborates Philander's (Philander, 1976, 1978) description of tropical instabilities naturally occurring at the Equator by the beta effect: eastward zonal fluxes tend to be naturally stable, and westward fluxes tend to be unstable because of the Coriolis effect. The spectral analysis for the indexes boxes showed that although the strongest peak is the annual cycle (~360 days), periodicities of ~180 and ~120 days are also important. However, the coupling of these modes and how they occur within a year were not investigated. The results shown in this paper suggest that further investigation is needed to understand how TIWs contribute to the equatorial dynamics of the Atlantic Ocean.

references

An Soon-II: Interannual variations of the tropical ocean instability wave and ENSO, J. Clim., 21(15), 3680–3686, doi:10.1175/2008JCLI1701.1, 2008.

Athie, G. and Marin, F.: Cross-equatorial structure and temporal modulation of intraseasonal variability at the surface of the Tropical Atlantic Ocean, J. Geophys. Res., 113(C8), C08020, doi:10.1029/2007JC004332, 2008.

Baturin, N. G. and Niiler, P. P.: Effects of instability waves in the mixed layer of the equatorial Pacific, J. Geophys. Res., 102793(15), 771–27, doi:10.1029/97JC02455, 1997.

Bunge, L., Provost, C. and Kartavtseff, A.: Variability in horizontal current velocities in the central and eastern equatorial Atlantic in 2002, J. Geophys. Res., 112(C2), C02014, doi:10.1029/2006JC003704, 2007.

Caltabiano, A. C. V, Robinson, I. S. and Pezzi, L. P.: Multi-year satellite observations of instability waves in the Tropical Atlantic Ocean, Ocean Sci., 1, 97–112 [online] Available from: www.ocean-science.net/os/1/97/ (Accessed 8 November 2016), 2005.

Carton, J. A. and Giese, B. S.: A Reanalysis of Ocean Climate Using Simple Ocean Data Assimilation (SODA), Mon. Weather Rev., 136(8), 2999–3017, doi:10.1175/2007MWR1978.1, 2008.

Challenor, P. G., Cipollini, P., Cromwell, D., Challenor, P. G., Cipollini, P. and Cromwell, D.: Use of the 3D Radon Transform to Examine the Properties of Oceanic Rossby Waves, J. Atmos. Ocean. Technol., 18(9), 1558–1566, doi:10.1175/1520-0426(2001)018<1558:UOTRTT>2.0.CO;2, 2001.

Chelton, D. B., Wentz, F. J., Genremann, C. L., De Szoeke, R. A. and Schlax, M. G.: Satellite Microwave SST Observations of Transequatorial Tropical Instability Waves, Geophys. Res. Lett., 27(1), 1239–1242, doi:10.1029/1999GL011047, 2000.

Cox, M. D.: Generation and Propagation of 30-Day Waves in a Numerical Model of the Pacific, J. Phys. Oceanogr., 10(8), 1168–1186, doi:10.1175/1520-0485(1980)010<1168:GAPODW>2.0.CO;2, 1980.

Czeschel, R., Stramma, L., Schwarzkopf, F. U., Giese, B. S., Funk, A. and Karstensen, J.: Middepth circulation of the eastern tropical South Pacific and its link to the oxygen minimum zone, J. Geophys. Res., 116, doi:C01015\r10.1029/2010jc006565, 2011.

Davey, M. K., Huddleston, M., Sperber, K. R., Braconnot, P., Bryan, F., Chen, D., Colman, R. A., Cooper, C., Cubasch, U., Delecluse, P., Dewitt, D., Fairhead, L., Flato, G., Gordon, C., Hogan, T., Ji, M., Kimoto, M., Kitoh, A., Knutson, T. R., Latif, M., Le Treut, H., Li, T., Manabe, S., Mechoso, C. R., Meehl, G. A., Power, S. B., Roeckner, E., Terray, L., Vintzileos, A., Voss, R., Wang, B., Washington, W. M., Yoshikawa, I., Yu, J.-Y., Yukimoto, S. and Zebiak, S. E.: STOIC: a study of coupled model climatology and variability in tropical ocean regions, , doi:10.1007/s00382-001-0188-6, 2000.

Deans, S. R.: The Radon Transform and some of its applications, John Wiley&Sons, New York., 1983.

Decco, H. T. de: Ondas de Instabilidade Tropical no Oceano Atlântico: uma abordagem sinótica utilizando dados de modelagem oceânica, Universidade Federal do Rio de Janeiro., 2011.

Dewitte, B., Purca, S., Illig, S., Renault, L. and Giese, B. S.: Low-frequency modulation of intraseasonal equatorial Kelvin wave activity in the Pacific from SODA: 1958-2001, J. Clim., 21(22), 6060–6069, doi:10.1175/2008JCLI2277.1, 2008.

Du, Y. and Qu, T.: Three inflow pathways of the Indonesian throughflow as seen from the simple ocean data assimilation, Dyn. Atmos. Ocean., 50(2), 233–256, doi:10.1016/j.dynatmoce.2010.04.001, 2010.

Düing, W.: Review of the Equatorial Oceanographic Experiment, Bull. Am. Meteorol. Soc., 55(5), 398–404, doi:10.1175/1520-0477(1974)055<0398:ROTEOE>2.0.CO;2, 1974.

Düing, W., Hisard, P., Katz, E., Meincke, J., Miller, L., Moroshkin, K. V., Philander, G., Ribnikov, A. A., Voigt, K. and Weisberg, R.: Meanders and long waves in the equatorial Atlantic, Nature, 257(5524), 280–284, doi:10.1038/257280a0, 1975.

Farrar, J. T.: Barotropic Rossby Waves Radiating from Tropical Instability Waves in the Pacific Ocean, J. Phys. Oceanogr., 41(6), 1160–1181, doi:10.1175/2011JPO4547.1, 2011.

Fofonoff, N. P. and Millard, R. C.: Algorithms for computation of fundamental properties of seawater, UNESCO Tech. Pap.

Mar. Sci., 44, 53, doi:10.1111/j.1365-2486.2005.001000.x, 1983.

Grodsky, S. A., Carton, J. A., Provost, C., Servain, J., Lorenzzetti, J. A. and McPhaden, M. J.: Tropical instability waves at 0°N, 23°W in the Atlantic: A case study using Pilot Research Moored Array in the Tropical Atlantic (PIRATA) mooring data, J. Geophys. Res., 110(C8), C08010, doi:10.1029/2005JC002941, 2005.

Guiavarch, C., Treguier, A.-M. and Vangriesheim, A.: Deep currents in the Gulf of Guinea: along slope propagation of intraseasonal waves, Ocean Sci., 5(2), 141–153, 2009.

Ham, Y.-G. and Kang, I.-S.: Improvement of seasonal forecasts with inclusion of tropical instability waves on initial conditions, Clim. Dyn., 36(7–8), 1277–1290, doi:10.1007/s00382-010-0743-0, 2011.

Han, W., Webster, P. J., Lin, J.-L., Liu, W. T., Fu, R., Yuan, D., Hu, A., Han, W., Webster, P. J., Lin, J.-L., Liu, W. T., Fu, R., Yuan, D. and Hu, A.: Dynamics of Intraseasonal Sea Level and Thermocline Variability in the Equatorial Atlantic during 2002–03, J. Phys. Oceanogr., 38(5), 945–967, doi:10.1175/2008JPO3854.1, 2008.

Hinze, J. O.: Turbulence, McGraw-Hill., 1975.

Im, S.-H., An, S. Il, Lengaigne, M. and Noh, Y.: Seasonality of tropical instability waves and its feedback to the seasonal cycle in the tropical eastern Pacific., ScientificWorldJournal., 2012, 612048, doi:10.1100/2012/612048, 2012.

Imada, Y., Tatebe, H., Komuro, Y. and Kimoto, M.: Multi-Decadal Modulation of Tropical Pacific Instability Wave Activity since the Middle of the Twentieth Century, SOLA, 9(0), 102–105, doi:10.2151/sola.2013-023, 2013.

Jiang, C. L., Thompson, L. A., Kelly, K. A., Cronin, M. F., Jiang, C. L., Thompson, L. A., Kelly, K. A. and Cronin, M. F.: The Roles of Intraseasonal Kelvin Waves and Tropical Instability Waves in SST Variability along the Equatorial Pacific in an Isopycnal Ocean Model, J. Clim., 22(12), 3470–3487, doi:10.1175/2009JCLI2767.1, 2009.

Jochum, M. and Malanotte-Rizzoli, P.: A New Theory for the Generation of the Equatorial Subsurface Countercurrents, J. Phys. Oceanogr., 34(4), 755–771, doi:10.1175/1520-0485(2004)034<0755:ANTFTG>2.0.CO;2, 2004.

Jochum, M., Murtugudde, R., Malanotte-Rizzoli, P. and Busalacchi, A.: Internal variability of the Tropical Atlantic Ocean. In: Ocean-atmosphere interaction and climate variability, in Ocean-Atmosphere Interaction and Climate Variability, pp. 181–188., 2004a.

Jochum, M., Malanotte-Rizzoli, P. and Busalacchi, A.: Tropical instability waves in the Atlantic Ocean, Ocean Model., 7(1), 145–163, doi:10.1016/S1463-5003(03)00042-8, 2004b.

Johnson, D. E. Al: World Ocean Database 2005, Administrator, 164, doi:Available from http://www.nodc.noaa.gov/OC5/indprod.html, 2006.

Katz, E. J.: Waves along the Equator in the Atlantic*, 1997.

Lackmann, G. M., Keyser, D., Bosart, L. F., Lackmann, G. M., Keyser, D. and Bosart, L. F.: Energetics of an Intensifying Jet Streak during the Experiment on Rapidly Intensifying Cyclones over the Atlantic (ERICA), Mon. Weather Rev., 127(12), 2777–2795, doi:10.1175/1520-0493(1999)127<2777:EOAIJS>2.0.CO;2, 1999.

Lee, T., Lagerloef, G., Gierach, M. M., Kao, H. Y., Yueh, S. and Dohan, K.: Aquarius reveals salinity structure of tropical instability waves, Geophys. Res. Lett., 39(12), doi:10.1029/2012GL052232, 2012.

Legeckis, R. and Reverdin, G.: Long waves in the equatorial Atlantic Ocean during 1983, J. Geophys. Res., 92(C3), 2835, doi:10.1029/JC092iC03p02835, 1987.

Lyman, J. M., Johnson, G. C., Kessler, W. S., Lyman, J. M., Johnson, G. C. and Kessler, W. S.: Distinct 17- and 33-Day Tropical Instability Waves in Subsurface Observations*, J. Phys. Oceanogr., 37(4), 855–872, doi:10.1175/JPO3023.1, 2007.

Masina, S., Philander, S. G. H. and Bush, A. B. G.: An analysis of tropical instability waves in a numerical model of the Pacific Ocean: 2. Generation and energetics of the waves, J. Geophys. Res., 104(C12), 29637, doi:10.1029/1999JC900226, 1999.

Millero, F. J., Chen, C.-T., Bradshaw, A. L. and Schleicher, K.: A New High Pressure Equation of State for Seawater, Deep Sea Res. Part A. Oceanogr. Res. Pap., 27(3–4), 255–264, doi:10.1016/0198-0149(80)90016-3, 1980.

Monin, A. S., Yaglom, A. M. and Lumley, J. L.: Statistical Fluid Mechanics - vol 1: Mechanics of Turbulence: A. S. Monin,

A. M. Yaglom, John L. Lumley: 9780262130622: Amazon.com: Books, The MIT Press. [online] Available from: https://www.amazon.com/Statistical-Fluid-Mechanics-vol-Turbulence/dp/0262130629, 1971.

Orlanski, I. and Katzfey, J.: The life cycle of a cyclone wave in the Southern Hemisphere. Part I: eddy energy budget, J. Atmos. Sci., 48(17), 1972–1998, doi:10.1175/1520-0469(1991)048<1972:TLCOAC>2.0.CO;2, 1991.

Perez, R. C., Lumpkin, R., Johns, W. E., Foltz, G. R. and Hormann, V.: Interannual variations of Atlantic tropical instability waves, J. Geophys. Res., 117(January), 1–13, doi:10.1029/2011JC007584, 2012.

Pezzi, L. P. and Richards, K. J.: Effects of lateral mixing on the mean state and eddy activity of an equatorial ocean, J. Geophys. Res., 108(C12), 3371, doi:10.1029/2003JC001834, 2003.

Pezzi, L. P., Caltabiano, A. C. V and Challenor, P.: Satellite observations of the Pacific tropical instability wave characteristics and their interannual variability, Int. J. Remote Sens., 27(8), 1581–1599, doi:10.1080/01431160500380588, 2006.

Philander, S. G. H.: equatorial undercurrent: Measurements and theories, Rev. Geophys., 11(3), 513, doi:10.1029/RG011i003p00513, 1973.

Philander, S. G. H.: Instabilities of zonal equatorial currents, J. Geophys. Res., 81(21), 3725–3735, doi:10.1029/JC081i021p03725, 1976.

Philander, S. G. H.: The effects of coastal geometry on equatorial waves (Forced waves in the Gulf of Guinea), J. Mar. Res., 35(3), 509–523, 1977.

Philander, S. G. H.: Instabilities of zonal equatorial currents, 2, J. Geophys. Res., 83(C7), 3679, doi:10.1029/JC083iC07p03679, 1978.

Philander, S. G. H., Hurlin, W. J. and Pacanowski, R. C.: Properties of long equatorial waves in models of the seasonal cycle in the tropical Atlantic and Pacific Oceans, J. Geophys. Res., 91(C12), 14207, doi:10.1029/JC091iC12p14207, 1986.

Polito, P. S. and Sato, O. T.: Patterns of sea surface height and heat storage associated to intraseasonal Rossby waves in the tropics, J. Geophys. Res, 108(337310), doi:10.1029/2002JC001684, 1029.

Proehl, J. A.: The role of meridional flow asymmetry in the dynamics of tropical instability, J. Geophys. Res. Ocean., 103(C11), 24597–24618, doi:10.1029/98JC02372, 1998.

Qiao, L. and Weisberg, R. H.: Tropical instability wave kinematics: Observations from the Tropical Instability Wave Experiment, J. Geophys. Res., 100(C5), 8677, doi:10.1029/95JC00305, 1995.

Qiao, L. and Weisberg, R. H.: Tropical Instability Wave Energetics: Observations from the Tropical Instability Wave Experiment, J. Phys. Oceanogr., 28(2), 345–360, doi:10.1175/1520-0485(1998)028<0345:TIWEOF>2.0.CO;2, 1998.

Reynolds, O.: On the Dynamical Theory of Incompressible Viscous Fluids and the Determination of the Criterion, Philos. Trans. R. Soc. A Math. Phys. Eng. Sci., 186(0), 123–164, doi:10.1098/rsta.1895.0004, 1895.

Schoenefeldt, R. and Schott, F. A.: Decadal variability of the Indian Ocean cross-equatorial exchange in SODA, Geophys. Res. Lett., 33(8), doi:10.1029/2006GL025891, 2006.

von Schuckmann, K., Brandt, P. and Eden, C.: Generation of tropical instability waves in the Atlantic Ocean, J. Geophys. Res., 113(C8), C08034, doi:10.1029/2007JC004712, 2008.

Seo, H., Jochum, M., Murtugudde, R. and Miller, A. J.: Effect of ocean mesoscale variability on the mean state of tropical Atlantic climate, Geophys. Res. Lett., 33(9), L09606, doi:10.1029/2005GL025651, 2006.

Seo, H., Jochum, M., Murtugudde, R., Miller, A. J. and Roads, J. O: Feedback of Tropical Instability Wave-induced atmospheric variability onto the ocean, J. Climate, 20, doi:10.1175/2007JCLI1700.1, 2007.

Soon-II, A.: Interannual changes in the variability of tropical Pacific instability waves, Asia-Pacifc J. Atmos. Sci., 44(3), 249–258, 2008.

Steger, J. M. and Carton, J. A.: Long waves and eddies in the tropical Atlantic Ocean: 1984–1990, J. Geophys. Res., 96(C8), 15161, doi:10.1029/91JC01316, 1991.

Stramma, L. and Schott, F.: The mean flow field of the tropical Atlantic Ocean, Deep Sea Res. Part II Top. Stud. Oceanogr., 46(1), 279–303, doi:10.1016/S0967-0645(98)00109-X, 1999.

Weisberg, R. H.: Equatorial waves during GATE and their relation to the mean zonal circulation, Deep. Res., 26(Suppl. II), 179–198, 1979.

Weisberg, R. H.: Instability waves observed on the Equator in the Atlantic Ocean during 1983, Geophys. Res. Lett., 11(8), 753–756, doi:10.1029/GL011i008p00753, 1984.

Weisberg, R. H.: Equatorial Atlantic Velocity and Temperature Observations: February–November 1981, J. Phys. Oceanogr., 15(5), 533–543, doi:10.1175/1520-0485(1985)015<0533:EAVATO>2.0.CO;2, 1985.

Weisberg, R. H. and Horigan, A. M.: Low-frequency variability in the Equatorial Atlantic, J. Phys. Oceanogr., 11(7), 913–920, doi:10.1175/1520-0485(1981)011<0913:LFVITE>2.0.CO;2, 1981.

Weisberg, R. H. and Weingartner, T. J.: Instability Waves in the Equatorial Atlantic Ocean, J. Phys. Oceanogr., 18(11), 1641–1657, doi:10.1175/1520-0485(1988)018<1641:IWITEA>2.0.CO;2, 1988.

Weisberg, R. H., Horigan, A. and Colins, C.: Equatorially trapped Rossby-gravity wave propagation in the Gulf of Guinea Equatoridly trapped Wossby-gravity wave propagation in the Gulf of Guinea, , 37(1), 67–86, 1979.

ACKNOWLEDGMENTS

We thank Professor James Carton and his team for their diligent help with the SODA 5-day mean results.

APPENDIX

DERIVATION OF EDDY KINETIC ENERGY EQUATION

In this section the derivation of EKE equation is described under the approach adopted in the present study. As showed in equation (1), the perturbation field was defined to be the filtered TIW signal and the basic state, the difference between the total and perturbation fields (these fields are illustrated on Figure 4). This implies the consideration that the classically defined (time or space) mean state is now a transient variable. Orlanski and Katzfey (Orlanski and Katzfey, 1991)applied a transient basic (or “mean”, as Orlanski and Katzfey, (Orlanski and Katzfey, 1991), called) state to study the energy transferences between a synoptic fields and a cyclone. This was done by including a forcing term, responsible for the transience, on the EKE equation, with no interference on the terms of instability processes. Here reference is made to the EKE equation from the study of Masina et al. (Masina et al., 1999)who considered the classical assumption averaging the momentum equations applying it to TIWs in the Pacific.

Reynolds (Reynolds, 1895) defined, for the first time, the turbulence of a flow. His complete deduction was made based on observational experiment about the flow on a tube and then he was able to define all the assumptions necessary for his mathematical description and deduction of the turbulent kinetic energy equation within that closed system. With his concepts incorporated in fluid mechanics the turbulence is considered to be a measure of the instability of flows, being defined as a statistical quantity (Monin et al., 1971). It should never be intended to define exactly the dynamical field of determined turbulent scale, according to this definition. Instead, one can describe the patterns associated to that scale of some band in the spectral response. The reader is referred to Monin and Yaglon (Monin

et al., 1971) and Hinze (Hinze, 1975) for more details as classical texts in this subject. This approach was adopted in this study, in which TIWs patterns are briefly described as a spectral signature of 15-60 days of period and 4-20 longitude degrees of wavelength of the equatorial circulation, to revisit energy exchanges between related to TIWs. In the following, the derivation of EKE equation is described showing the considerations and scale analysis made in order to obtain a similar EKE equation of Orlanski and Katzfey (Orlanski and Katzfey, 1991) and Masina et al. (Masina et al., 1999).

The process involved on the derivation of a turbulent kinetic energy equation from the momentum equations is through Reynolds averaging (Hinze, 1975; Monin et al., 1971). The sequence of the following steps is showed below: i) definition of momentum equations; ii) flux (basic state and perturbation) decomposition; iii) Reynolds averaging; iv) Reynolds postulates and scale analysis for the current approach; iv) obtaining the momentum equation for the perturbation and v) obtaining of the EKE equation.

The total kinetic energy K is defined as follows:

$$K = \rho \frac{1}{2} \mathbf{v}^2 \qquad (2),$$

where **v** is the three-dimensional velocity field, $\mathbf{v} = u + v + w$, and ρ is the density of the fluid.

Applying flux decomposition (1) in Eq. (2):

$$K = \rho \frac{1}{2} \left(\mathbf{v}_b + \mathbf{v}' \right)^2 = \rho \frac{1}{2} \left(\mathbf{v}_b{}^2 + 2\mathbf{v}_b \mathbf{v}' + \mathbf{v}'^2 \right) \qquad (3),$$

where the first term on the right-hand side of Eq. (4) is the kinetic energy of the basic state (K_b), the second is the first-order correlation term (Orlanski and Katzfey, 1991) (K_1), and the last term is the kinetic energy of perturbation (K_e); in this case, it is assumed to be the TIWs.

The horizontal (Equations 4 and 5) and vertical (Equation 6) momentum equations in the Cartesian coordinates, under hydrostatic approximation, are written as follows:

$$\frac{Du}{Dt} - 2\Omega \sin\varphi v + 2\Omega \cos\varphi w = -\frac{1}{\rho_o} \frac{\partial p}{\partial x} + A_H \left(\frac{\partial^2 u}{\partial x^2} + \frac{\partial^2 u}{\partial y^2} \right) + A_Z \frac{\partial^2 u}{\partial z^2} \qquad (4),$$

$$\frac{Dv}{Dt} + 2\Omega \sin\varphi u = -\frac{1}{\rho_o} \frac{\partial p}{\partial y} + A_H \left(\frac{\partial^2 v}{\partial x^2} + \frac{\partial^2 v}{\partial y^2} \right) + A_Z \frac{\partial^2 v}{\partial z^2} \qquad (5),$$

$$\frac{\partial p}{\partial z} = -\rho_0 g \qquad (6),$$

where u, v and w are the total quantities of the zonal, meridional and vertical velocity components, respectively; $\frac{D}{Dt} = \frac{\partial}{\partial t} + u\frac{\partial}{\partial x} + v\frac{\partial}{\partial y} + w\frac{\partial}{\partial z}$ is the material derivative; $2\Omega \sin\varphi$ is the Coriolis parameter; p is the total field of pressure; ρ_0 is the reference density; A_H and A_Z are the horizontal and vertical eddy viscosities, respectively; and g is the acceleration due to gravity (9.81m/s²).

Applying the flux decomposition of Eq. (1) in Equations (4, 5 and 6), we obtain the following:

$$\frac{D(u_b+u')}{Dt} - 2\Omega\sin\varphi(v_b+v') + 2\Omega\cos\varphi(w_b+w') =$$

$$-\frac{1}{\rho_o}\frac{\partial(p_b+p')}{\partial x} + A_H\left(\frac{\partial^2(u_b+u')}{\partial x^2} + \frac{\partial^2(u_b+u')}{\partial y^2}\right) + A_Z\frac{\partial^2(u_b+u')}{\partial z^2} \quad (7),$$

$$\frac{D(v_b+v')}{Dt} + 2\Omega\sin\varphi(u_b+u') =$$

$$-\frac{1}{\rho_o}\frac{\partial(p_b+p')}{\partial y} + A_H\left(\frac{\partial^2(v_b+v')}{\partial x^2} + \frac{\partial^2(v_b+v')}{\partial y^2}\right) + A_Z\frac{\partial^2(v_b+v')}{\partial z^2} \quad (8),$$

$$\frac{\partial(p_b+p')}{\partial z} = -(\rho_0+\rho')g \quad (9).$$

In the next step, the temporal mean is applied to equations (7, 8 and 9) (for the sake of brevity, the derivation is subsequently only shown for the zonal velocity component):

$$\overline{\frac{\partial u_b}{\partial t}} + \overline{\frac{\partial u'}{\partial t}} + \left(\overline{u_b\frac{\partial u_b}{\partial x}} + \overline{u_b\frac{\partial u'}{\partial x}} + \overline{u'\frac{\partial u_b}{\partial x}} + \overline{u'\frac{\partial u'}{\partial x}}\right) + \left(\overline{v_b\frac{\partial u_b}{\partial y}} + \overline{v_b\frac{\partial u'}{\partial y}} + \overline{v'\frac{\partial u_b}{\partial y}} + \overline{v'\frac{\partial u'}{\partial y}}\right)$$

$$+\left(\overline{w_b\frac{\partial u_b}{\partial z}} + \overline{w_b\frac{\partial u'}{\partial z}} + \overline{w'\frac{\partial u_b}{\partial z}} + \overline{w'\frac{\partial u'}{\partial z}}\right) = 2\Omega\sin\varphi(\overline{v_b+v'}) - 2\Omega\cos\varphi\left(\overline{w_b+w'}\right)$$

$$-\frac{1}{\rho_o}\overline{\frac{\partial p_b}{\partial x}} - \frac{1}{\rho_o}\overline{\frac{\partial p'}{\partial x}} + A_H\left(\overline{\frac{\partial^2(u_b+u')}{\partial x^2}} + \overline{\frac{\partial^2(u_b+u')}{\partial y^2}}\right) + A_Z\overline{\frac{\partial^2(u_b+u')}{\partial z^2}} \quad (10),$$

where an overbar is used to indicate the time mean and the time mean and the Coriolis terms have been moved to the right hand side of the equation.

The basic state defined in this study implies in distinct assumptions related to the Reynolds postulates (Orlanski and Katzfey, 1991). Also a scalar analysis for each of the postulates listed in the following was performed to confirm that each of that was null (or almost zero) using the results calculated with SODA. Only one postulate was considered to be different for the present case:

$$\overline{\phi_b} \neq \phi_b \quad (11),$$

where ϕ is any property studied here. When this postulate is applied, Eq. (10) becomes the following:

$$\overline{u_b\frac{\partial u_b}{\partial x}} + \overline{v_b\frac{\partial u_b}{\partial y}} + \overline{w_b\frac{\partial u_b}{\partial z}} + \overline{u'\frac{\partial u'}{\partial x}} + \overline{v'\frac{\partial u'}{\partial y}} + \overline{w'\frac{\partial u'}{\partial z}}$$

$$= 2\Omega\sin\varphi\overline{v_b} - 2\Omega\cos\varphi\overline{w_b} - \frac{1}{\rho_o}\overline{\frac{\partial p_b}{\partial x}} + A_H\left(\overline{\frac{\partial^2 u_b}{\partial x^2}} + \overline{\frac{\partial^2 u_b}{\partial y^2}}\right) + A_Z\overline{\frac{\partial^2 u_b}{\partial z^2}} \quad (12),$$

Finally, the total momentum (with flux decomposition) Eq. (7) minus Eq. (12) provides the momentum equation for the perturbations (TIWs), which, after neglecting any terms related to the basic state that do not influence TIWs, becomes the following:

$$\left(\frac{\partial u'}{\partial t} + u_b\frac{\partial u'}{\partial x} + v_b\frac{\partial u'}{\partial y} + w_b\frac{\partial u'}{\partial z}\right) + \left(u'\frac{\partial u'}{\partial x} + v'\frac{\partial u'}{\partial y} + w'\frac{\partial u'}{\partial z}\right) + \left(u'\frac{\partial u_b}{\partial x} + v'\frac{\partial u_b}{\partial y} + w'\frac{\partial u_b}{\partial z}\right)$$

$$-\left(\overline{u'\frac{\partial u'}{\partial x}}+\overline{v'\frac{\partial u'}{\partial y}}+\overline{w'\frac{\partial u'}{\partial z}}\right)=2\Omega\sin\varphi v'-2\Omega\cos\varphi w'-\frac{1}{\rho_o}\frac{\partial p'}{\partial x}$$

$$+A_H\left(\frac{\partial^2 u'}{\partial x^2}+\frac{\partial^2 u'}{\partial y^2}\right)+A_Z\frac{\partial^2 u'}{\partial z^2} \qquad (13).$$

The EKE equation is then obtained after a scalar multiplication of Eq. (13) by the TIW zonal velocity component, which yields the identical EKE equation of Orlanski and Katzfey (Orlanski and Katzfey, 1991)and Masina et al. (Masina et al., 1999). This result shows that although a distinct flux decomposition approach is used, it is possible to study TIWs and the basic circulation energy exchanges using the classical equation for EKE. Then, considering K_e as ($u'u'+v'v'$), the total EKE equation becomes:

$$\left(\frac{\partial K_e}{\partial t}+u_b\frac{\partial K_e}{\partial x}+v_b\frac{\partial K_e}{\partial y}+w_b\frac{\partial K_e}{\partial z}\right)+\left(u'\frac{\partial K_e}{\partial x}+v'\frac{\partial K_e}{\partial y}+w'\frac{\partial K_e}{\partial z}\right)$$

$$=\rho_0\left[-u'\left(u'\frac{\partial u_b}{\partial x}+v'\frac{\partial u_b}{\partial y}+w'\frac{\partial u_b}{\partial z}\right)-v'\left(u'\frac{\partial v_b}{\partial x}+v'\frac{\partial v_b}{\partial y}+w'\frac{\partial v_b}{\partial z}\right)...\right]$$

$$\left[...+u'\left(\overline{u'\frac{\partial u'}{\partial x}}+\overline{v'\frac{\partial u'}{\partial y}}+\overline{w'\frac{\partial u'}{\partial z}}\right)+v'\left(\overline{u'\frac{\partial v'}{\partial x}}+\overline{v'\frac{\partial v'}{\partial y}}+\overline{w'\frac{\partial v'}{\partial z}}\right)...\right]$$

$$\left[...+u'\left(A_H\left(\frac{\partial^2 u'}{\partial x^2}+\frac{\partial^2 u'}{\partial y^2}\right)+A_Z\left(\frac{\partial^2 u'}{\partial z^2}\right)\right)+v'\left(A_H\left(\frac{\partial^2 v'}{\partial x^2}+\frac{\partial^2 v'}{\partial y^2}\right)+A_Z\left(\frac{\partial^2 v'}{\partial z^2}\right)\right)\right]$$

$$+2\Omega\sin\varphi v'u'-2\Omega\cos\varphi w'u'-2\Omega sen\varphi u'v$$

$$+\left(-u'\frac{\partial p'}{\partial x}-v'\frac{\partial p'}{\partial y}-w'\frac{\partial p'}{\partial z}-g\rho' w'\right) \qquad (14).$$

The left-hand side terms in Eq. (14) are the local tendency and total advection of K_e by the basic state and TIW circulation, respectively. The first line on the right-hand side of Eq. (14) is the energy conversion by the Reynolds stresses, which is considered to be the transfer between the basic state and TIWs. The second line represents the divergence of K_e by TIWs. In the time-dependent evolution, the energy transfer involves a transition term, the first-order correlation term of Eq. (3) (Orlanski and Katzfey, 1991). This term is considered by Orlanski and Katzfey (Orlanski and Katzfey, 1991) as being another transition level of energy transference, and they considered these two terms of transition to be zero relative to the time mean and are also valid here. The eddy dissipation is represented by the third line. In the following, the fourth line the terms of Coriolis influence on the eddy velocity field. The last four terms represent the pressure work divergence done by TIWs, which are written under hydrostatic pressure approximation, and are responsible for the spatial redistribution of K_e (more details can be found in Masina et al. (Masina et al., 1999).

The horizontal and vertical deformation terms in Eq. (14) provided by the first term on the right-hand side are known as the barotropic and Kelvin-Helmholtz energy conversions, respectively. These terms represent the generation of TIW kinetic energy, as an interaction of Reynolds stresses with the basic state components. When these terms are positive, they are considered to be conversions of basic state kinetic energy into TIW kinetic energy as a result of horizontal and vertical flow shears, respectively.

The baroclinic conversion is provided by the last term in Eq. (14). This term is responsible for the conversion of basic state available potential energy to TIW kinetic energy (if positive) through vertical deformation work.

TABLES

Table 1. Dominant spectral characteristics of TIWs at 0.25ºN

	Satellite SST			SODA		
Year	Wavelength (degrees)	Period (days)	Wave Speed (cm/s)	Wavelength (degrees)	Period (days)	Wave Speed (cm/s)
2003	8	40	44	10	30	52
2004	7	24	39	8	24	34
2005	7	33	38	10	40	26
2006	7	24	42	6	28	35
2007	8	26	48	10	26	50
2008	7	33	41	8	30	34
mean	7.33	30	42	8.66	29.66	38.5

FIGURE CAPTION LIST

Figure 1: Sea surface temperature (SST) in the equatorial Atlantic Ocean (in ºC). (a) Merged Tropical Rainfall Measuring Mission Microwave Imager (TMI) and Advanced Microwave Scanning Radiometer (AMSR-E) SST from the Remote Sensing Systems project, 5-day mean from August 12 to 17, 2006; (b) SODA 2.1.6 temperature field mean in the first vertical model layer from August 12 to 17, 2006, with divisions illustrating the index regions: Eastern (EI), Western 1 (W1I), Western 2 (W2I) and Western 3 (W3I) indexes.

Figure 2: The power spectrum of temperature in the first vertical model layer at 0.75ºN–20.25ºW of the SODA 5-day total (a) and basic (b) states and TIWs (c).

Figure 3: Time-longitude plots of filtered sea surface temperature (ºC) at 0.25ºN. (a) daily TMI; (b) 5-day mean SODA; (c) daily TMI (color) and 5-day mean SODA (black contour) superposition for 2003.

Figure 4: Maps of the total and basic state and TIW anomaly fields (left, middle and right panels, respectively) from the SODA results in the first vertical model layer from August 12 to 17, 2006. (a), (b) and (c) The temperatures in ºC; (d), (e) and (f) salinity; (g), (h) and (i) zonal velocity; (j), (k) and (l) meridional velocity; (m), (n) and (o) vertical velocity (m/s).

Figure 5: Maps of the standard deviations of TIW anomaly fields of temperature in ºC (a), salinity (b), zonal, meridional and vertical velocity components in m/s (c, d and e, respectively) and sea surface elevation in m (f).

Figure 6: Time series of TIW EKE at 0.25ºN/28.25ºW, averaged on 5 meters depth (first vertical model layer), extracted from the SODA 5-day mean. The units are ergs/cm^3.

Figure 7: Maps of the mean TIW EKE averaged over three months: Jan-Feb-Mar (a), Apr-May-Jun (b), Jul-Aug-Sep (c), Oct-Nov-Dec (d). The units are ergs/cm^3.

Figure 8: Maps of the EKE standard deviations averaged over three months: Jan-Feb-Mar (a), Apr-May-Jun (b), Jul-Aug-Sep (c), Oct-Nov-Dec (d). The units are ergs/cm^3.

Figure 9: Energy spectra for the index time series of temperature (a), salinity (b), zonal (c) and meridional (d) velocity components (in the first vertical model layer) and sea surface elevation (e). Blue line is East Index, red line is West 1 Index, black line is West 2 Index and magenta line is West 3 Index.

Figure 10: Maps of time mean (a) and standard deviations (b) of barotropic energy conversion rates, time-mean (c) and standard deviations (d) of Kelvin-Helmholtz energy conversion rates and time-mean (e) and standard deviations (f) of baroclinic energy conversion rates. The units are in W/m³.

Figure 11: Energy spectra for the index time series of barotropic (a), Kelvin-Helmholtz (b) and baroclinic (c) energy conversions. Blue line is East Index, red line is West 1 Index, black line is West 2 Index and magenta line is West 3 Index. The units are in W/m³/day.

FIGURES

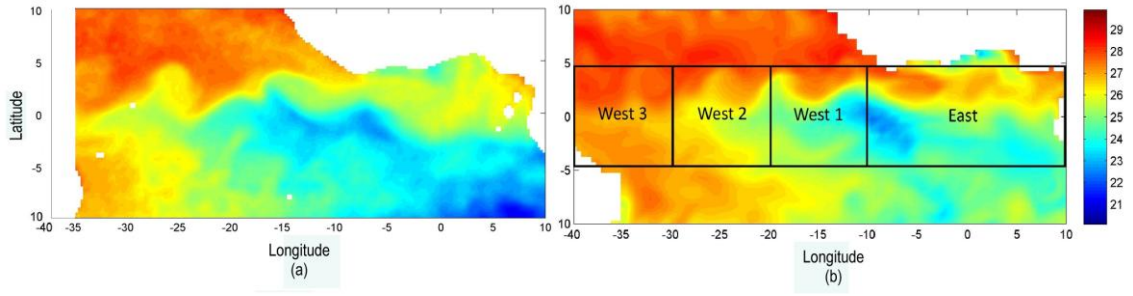

Figure 1: Sea surface temperature (SST) in the equatorial Atlantic Ocean (in ºC). (a) Merged Tropical Rainfall Measuring Mission Microwave Imager (TMI) and Advanced Microwave Scanning Radiometer (AMSR-E) SST from the Remote Sensing Systems project, 5-day mean from August 12 to 17, 2006; (b) SODA 2.1.6 temperature field mean in the first vertical model layer from August 12 to 17, 2006, with divisions illustrating the index regions: Eastern (EI), Western 1 (W1I), Western 2 (W2I) and Western 3 (W3I) indexes.

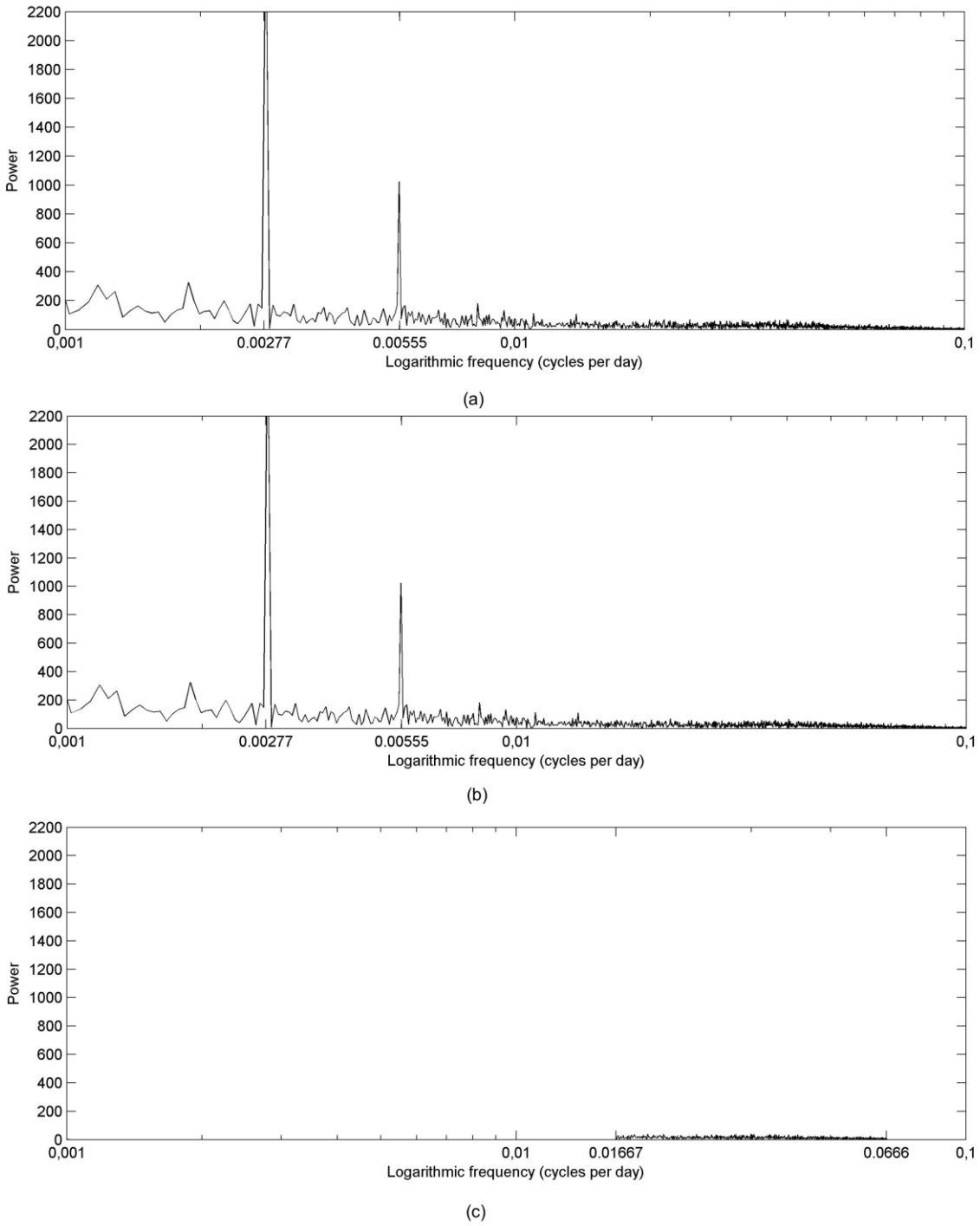

Figure 2: The power spectrum of temperature in the first vertical model layer at 0.75ºN–20.25ºW of the SODA 5-day total (a) and basic (b) states and TIWs (c).

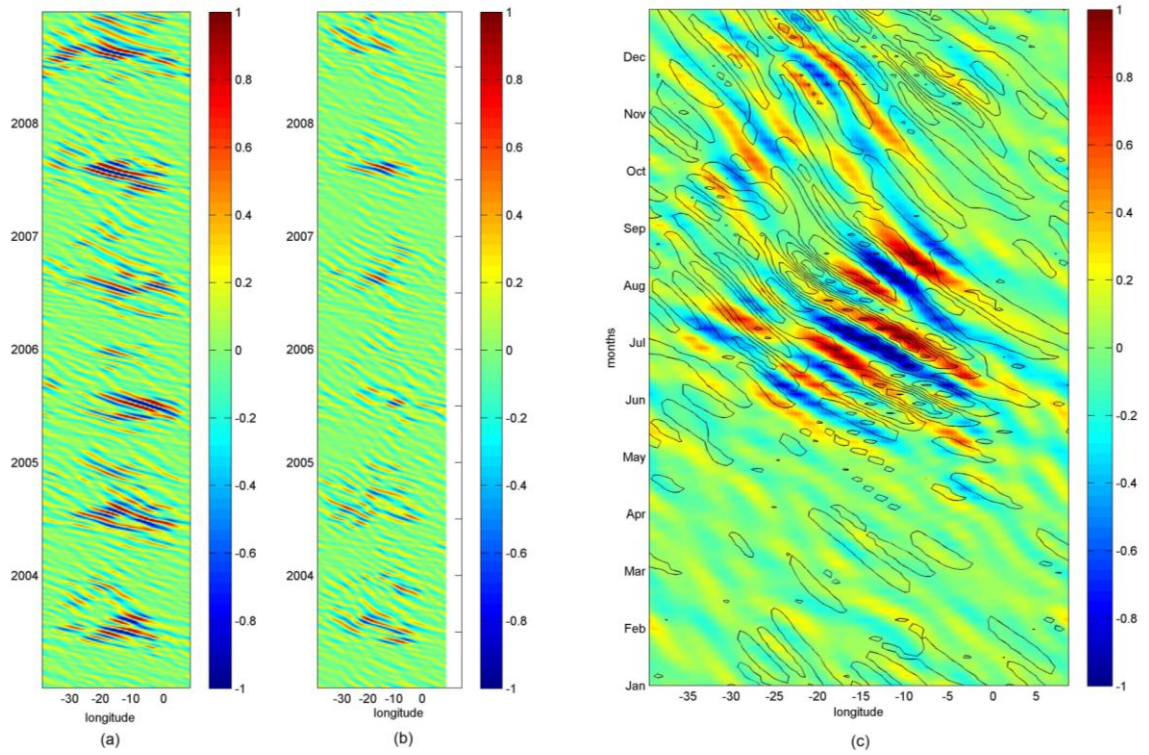

Figure 3: Time-longitude plots of filtered sea surface temperature (ºC) at 0.25ºN. (a) daily TMI; (b) 5-day mean SODA; (c) daily TMI (color) and 5-day mean SODA (black contour) superposition for 2003.

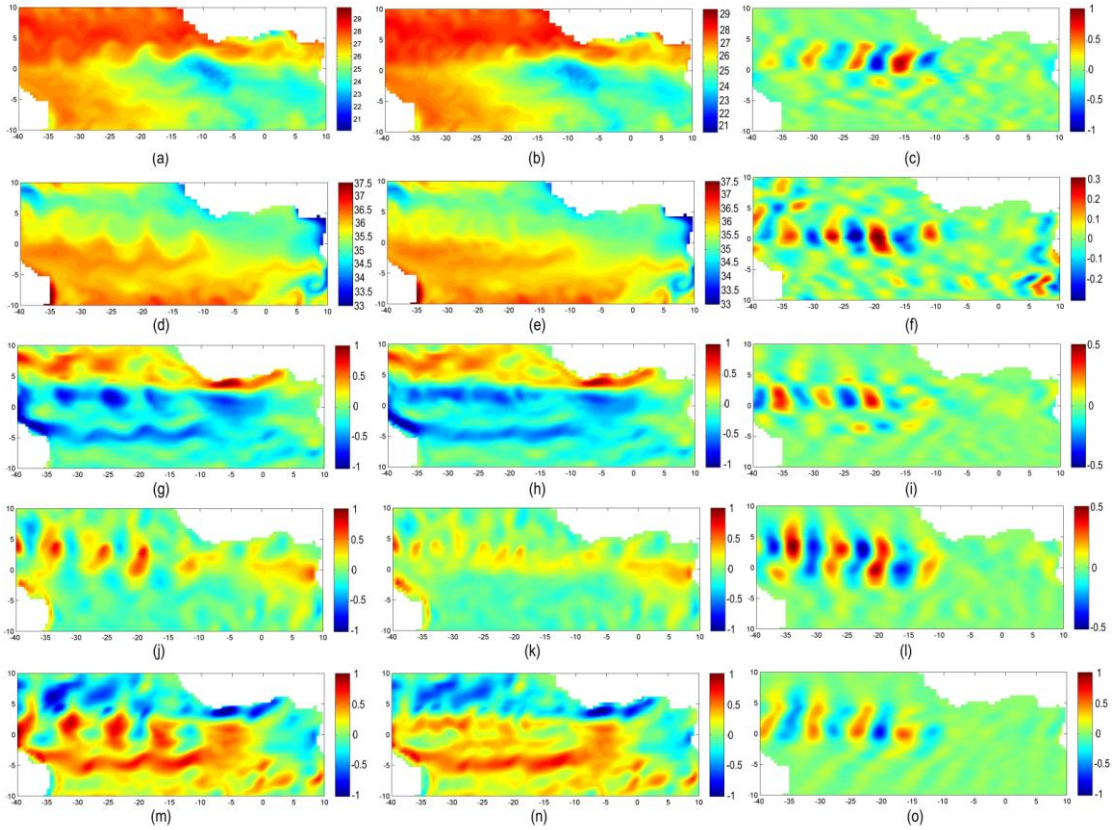

Figure 4: Maps of the total and basic state and TIW anomaly fields (left, middle and right panels, respectively) from the SODA results in the first vertical model layer from August 12 to 17, 2006. (a), (b) and (c) The temperatures in ºC; (d), (e) and (f) salinity; (g), (h) and (i) zonal velocity; (j), (k) and (l) meridional velocity; (m), (n) and (o) vertical velocity (m/s).

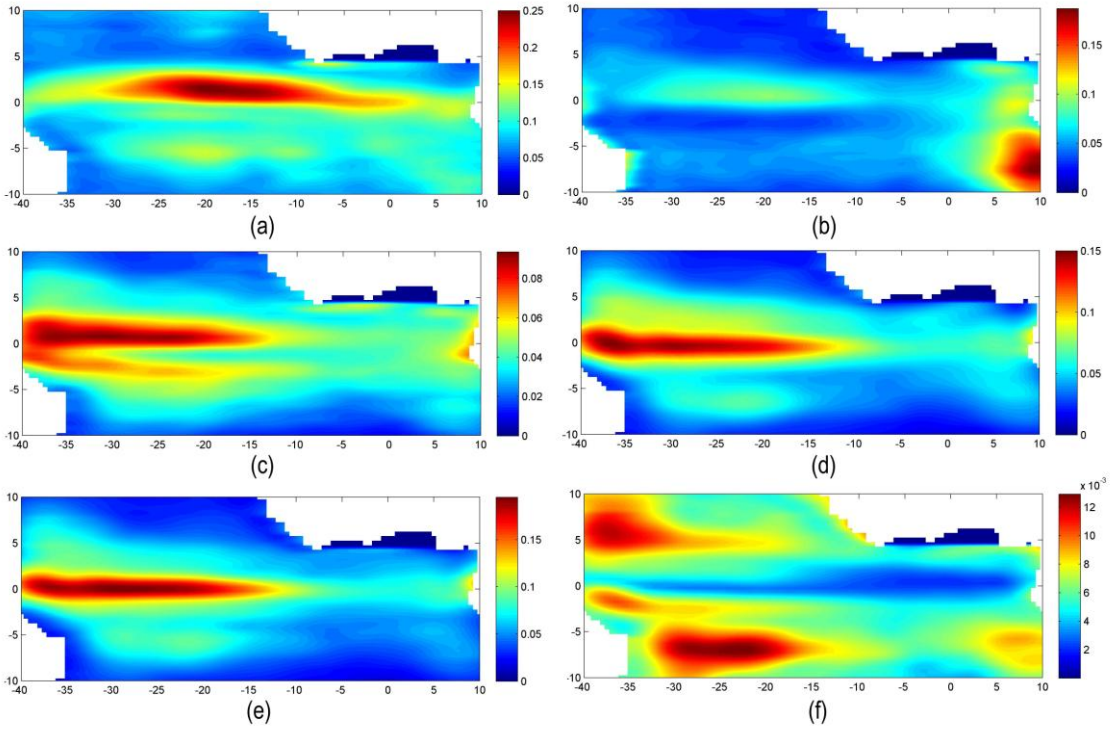

Figure 5: Maps of the standard deviations of TIW anomaly fields of temperature in ºC (a), salinity (b), zonal, meridional and vertical velocity components in m/s (c, d and e, respectively) and sea surface elevation in m (f).

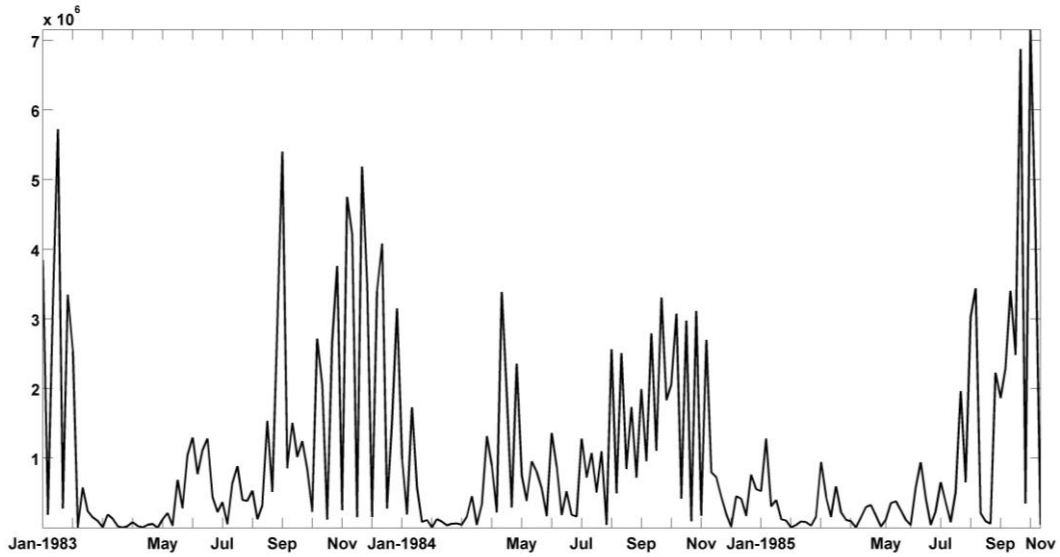

Figure 6: Time series of TIW EKE at 0.25ºN/28.25ºW, averaged on 5 meters depth (first vertical model layer), extracted from the SODA 5-day mean. The units are ergs/cm^3.

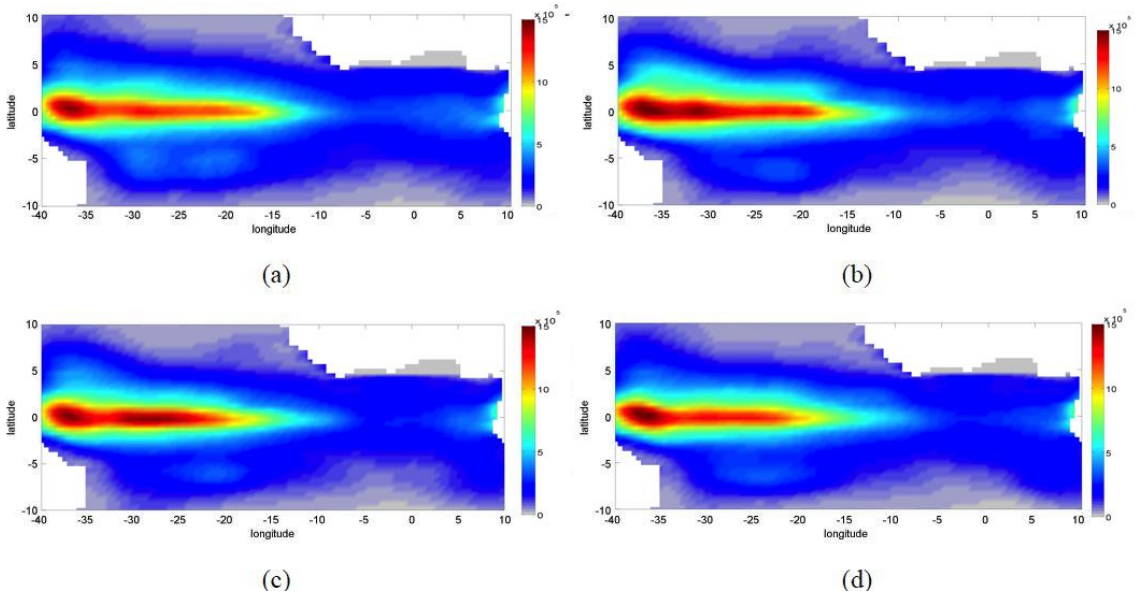

Figure 7: Maps of the mean TIW EKE averaged over three months: Jan-Feb-Mar (a), Apr-May-Jun (b), Jul-Aug-Sep (c), Oct-Nov-Dec (d). The units are ergs/cm^3.

825

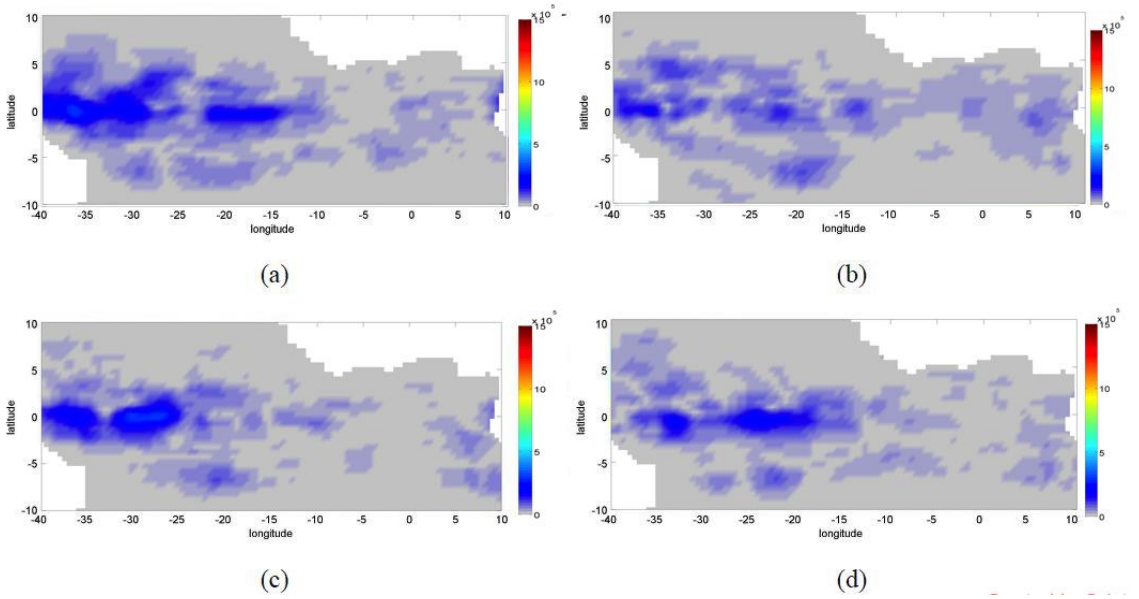

Figure 8: Maps of the EKE standard deviations averaged over three months: Jan-Feb-Mar (a), Apr-May-Jun (b), Jul-Aug-Sep (c), Oct-Nov-Dec (d). The units are ergs/cm^3.

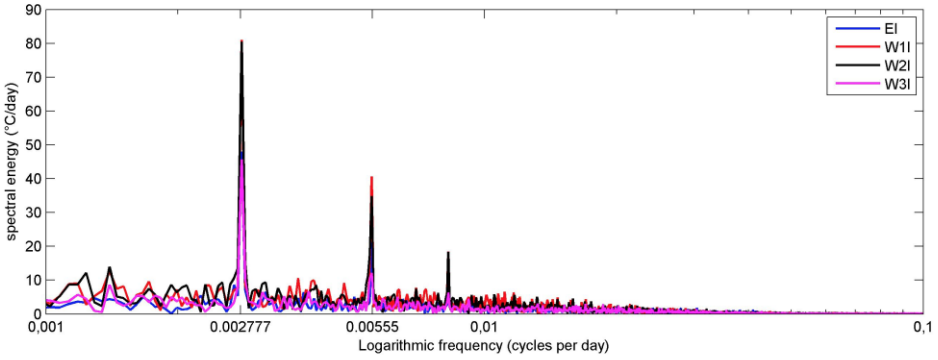
spectral energy (°C/day)
Logarithmic frequency (cycles per day)
0,001
0.002777
0.00555
0,01
0,1
EI
W1I
W2I
W3I

(a)

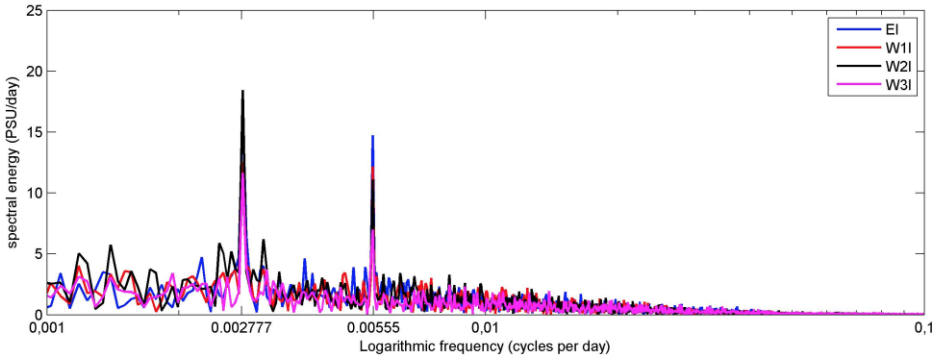
spectral energy (PSU/day)
Logarithmic frequency (cycles per day)
0,001
0.002777
0.00555
0,01
0,1
EI
W1I
W2I
W3I

(b)

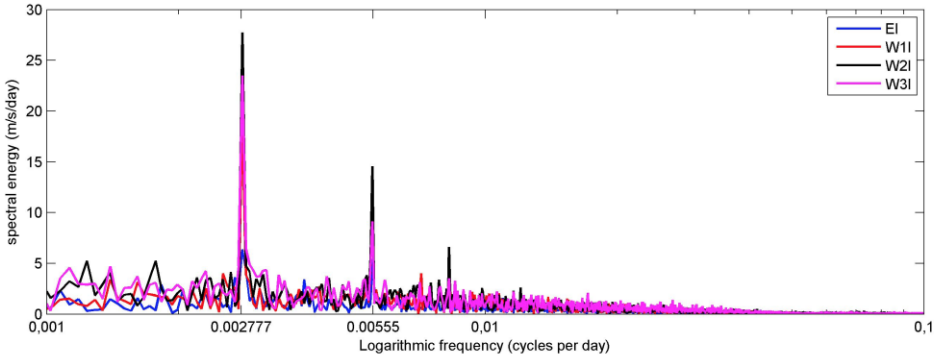
spectral energy (m/s/day)
Logarithmic frequency (cycles per day)
0,001
0.002777
0.00555
0,01
0,1
EI
W1I
W2I
W3I

(c)

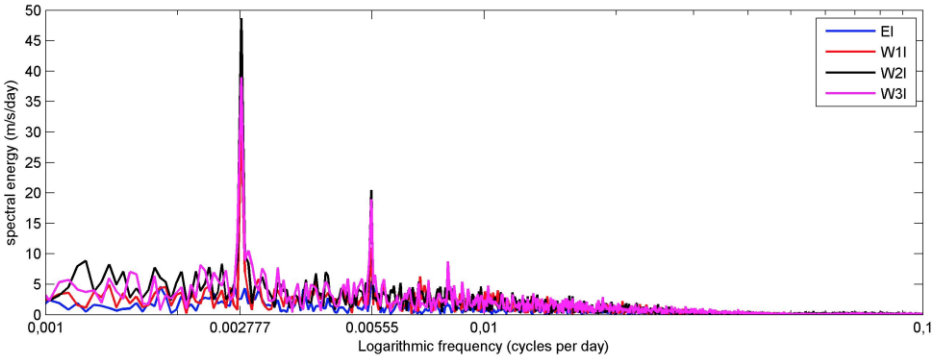
spectral energy (m/s/day)
Logarithmic frequency (cycles per day)
0,001
0.002777
0.00555
0,01
0,1
EI
W1I
W2I
W3I

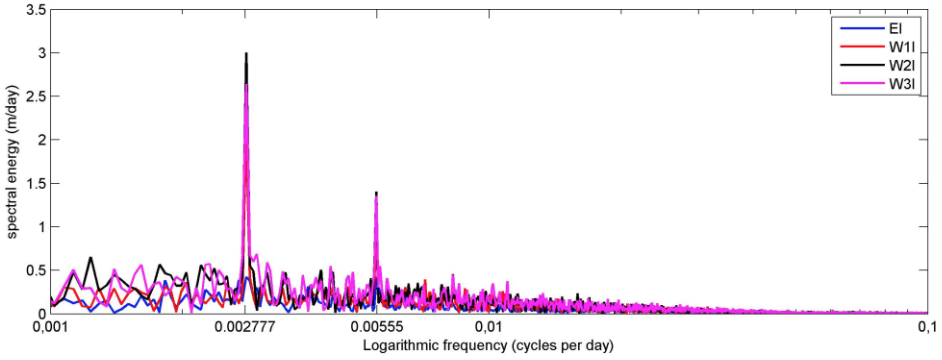
spectral energy (m/day)
Logarithmic frequency (cycles per day)
0,001
0.002777
0.00555
0,01
0,1
EI
W1I
W2I
W3I

(e)

Figure 9: Energy spectra for the index time series of temperature (a), salinity (b), zonal (c) and meridional (d) velocity components (in the first vertical model layer) and sea surface elevation (e). Blue line is East Index, red line is West 1 Index, black line is West 2 Index and magenta line is West 3 Index.

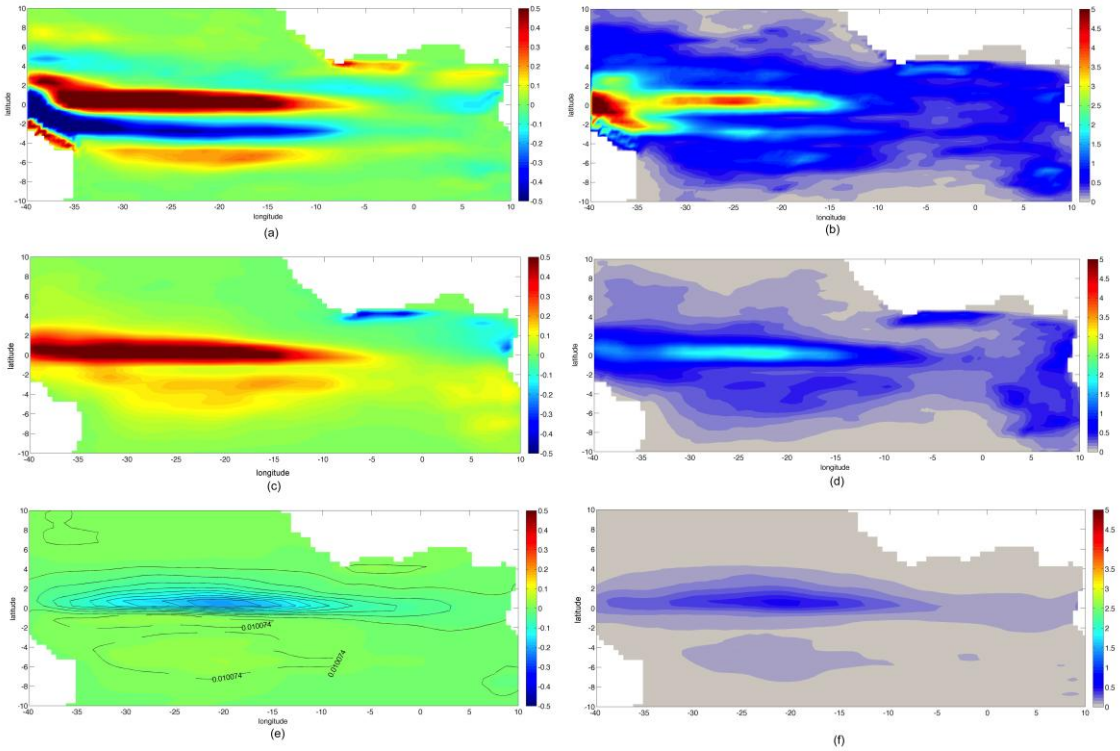

Figure 10: Maps of time mean (a) and standard deviations (b) of barotropic energy conversion rates, time-mean (c) and standard deviations (d) of Kelvin-Helmholtz energy conversion rates and time-mean (e) and standard deviations (f) of baroclinic energy conversion rates. The units are in W/m³.

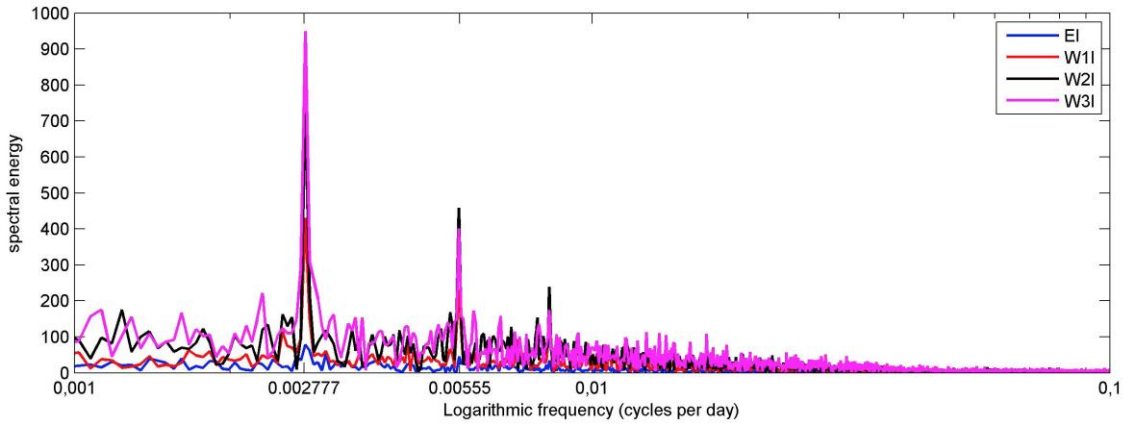

(a)

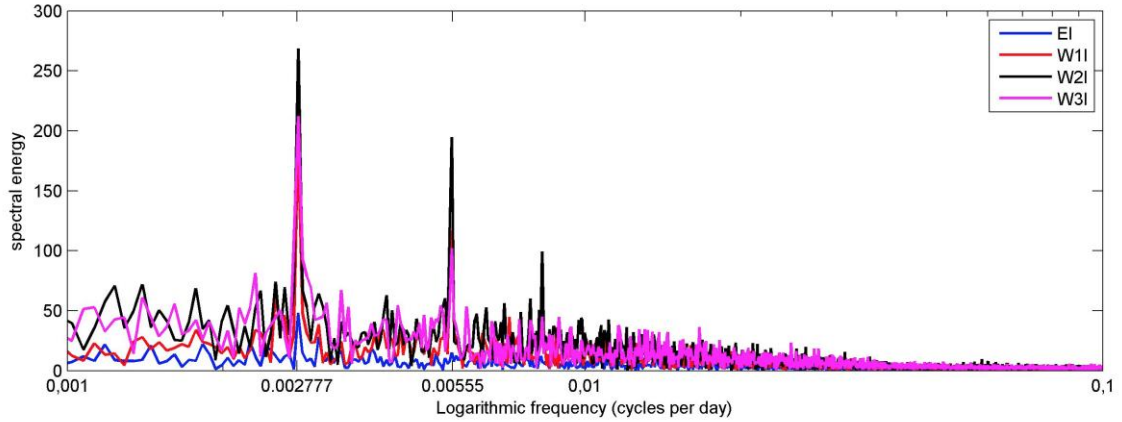

(b)

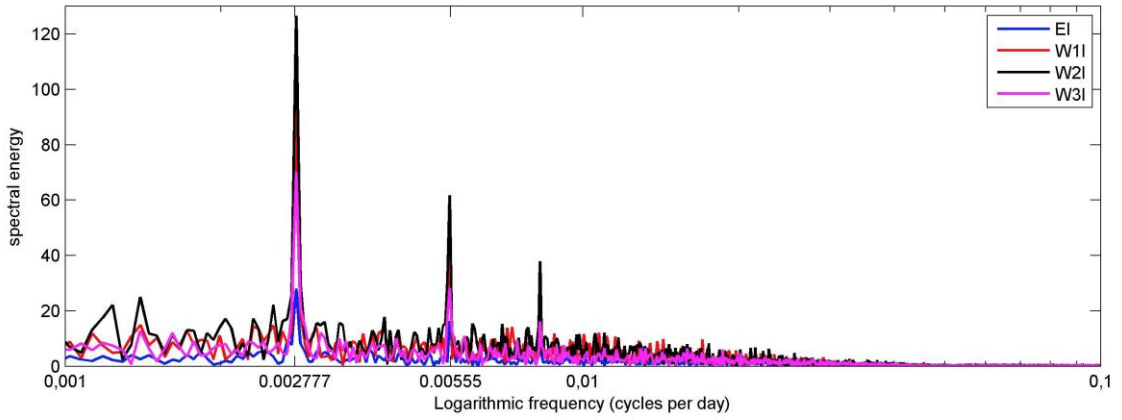

(c)

Figure 11: Energy spectra for the index time series of barotropic (a), Kelvin-Helmholtz (b) and baroclinic (c) energy conversions. Blue line is East Index, red line is West 1 Index, black line is West 2 Index and magenta line is West 3 Index. The units are in W/m³/day.